Dendrite branching receptor HPO-30 uses two novel mechanisms to regulate actin cytoskeletal remodeling

Daniel A. Kramer[1], Heidy Y. Narvaez-Ortiz[2], Julien Roche[1], Brad J. Nolen[2], and Baoyu Chen[1#]

Affiliations:

[1]Roy J Carver Department of Biochemistry, Biophysics, and Molecular Biology, Iowa State University, Ames, IA, 50014, USA.

[2]Department of Chemistry and Biochemistry, Institute of Molecular Biology, University of Oregon, Eugene, OR 97403, USA.

[#]Correspondence to: stone@iastate.edu

Abstract

Dendrite morphogenesis is essential to neural circuit formation, but the molecular mechanisms that control the growth of complicated dendrite branches are not well understood. Prior studies using the *C. elegans* PVD sensory neuron identified a multi-protein signaling complex that bridges extracellular cues with intracellular actin remodeling to promote high-order dendrite branching. In this complex, the transmembrane protein HPO-30 recruits the WAVE Regulatory Complex (WRC) to dendrite branching sites, where WRC stimulates the Arp2/3 complex to polymerize actin. Here we report biochemical and structural characterization of this interaction, revealing that the intracellular domain (ICD) of HPO-30 uses two novel mechanisms to regulate the actin cytoskeleton. First, the unstructured HPO-30 ICD undergoes dimerization and folding into a three-dimensional structure in order to bind the WRC. Second, the HPO-30 ICD directly binds to actin filaments, which stabilizes actin structures by preventing both actin polymerization and depolymerization. The novel dual functions of this dendrite receptor provide an intriguing example of how membrane proteins can use different mechanisms to locally fine-tune actin dynamics.

28 **Introduction**

29 While neurons have vastly different shapes, they all share a similar architecture—a cell
30 body, a long primary axon, and many branching protuberances called dendrites, along which are
31 many micron-sized projections called spines (Burianek and Soderling, 2013; Jan and Jan, 2003;
32 Lefebvre et al., 2015). The formation of dendrite branches and spines is critical for the
33 development of complex neuronal circuits, as they form the majority of post-synaptic
34 connections in animals and make up much of the brain volume, dictating brain function
35 (Hotulainen and Hoogenraad, 2010; Scott and Luo, 2001; Tavosanis, 2012). Dendrite
36 development requires actin and microtubule filaments to drive the initiation and outgrowth of
37 newly formed neurites (Cheng and Poo, 2012; Zhao et al., 2017). Defects in actin regulation alter
38 dendrite morphology and neural connections and contribute to many neurodevelopmental
39 disorders, such as autism, mental retardation, schizophrenia, and Alzheimer's (Yan et al., 2016).

40 A central mechanism by which cells control actin polymerization is through the Arp2/3
41 complex, a seven-protein complex that binds to the sides of existing actin filaments and
42 generates branched actin filament networks (Goley and Welch, 2006; Machesky et al., 1994;
43 Pollard, 2007). Intrinsically inactive, the Arp2/3 complex requires activation by a group of
44 proteins called nucleation promoting factors (NPFs). The Wiskott-Aldrich Syndrome Protein
45 (WASP) family proteins are major NPFs (Alekhina et al., 2017; Pollitt and Insall, 2009;
46 Takenawa and Suetsugu, 2007). They all contain a conserved WCA (WH2-central-acidic)
47 sequence at their C terminus (Machesky and Insall, 1998), which can directly bind to and
48 activate Arp2/3, while their N-terminal sequences vary greatly and define their regulatory
49 mechanism and cellular function (Alekhina et al., 2017).

50 Among the WASP-family proteins, WAVE (Wiskott-Aldrich Verprolin homology) exists
51 in a multi-protein complex named the WAVE Regulatory Complex (WRC), which contains five
52 subunits: Sra1, Nap1, Abi2, HSPC300, and WAVE (or their corresponding orthologs in
53 vertebrates) (Chen et al., 2010a; Eden et al., 2002; Gautreau et al., 2004; Polesskaya et al., 2021;
54 Rottner et al., 2021). Enriched in neurons, WRC and Arp2/3 promote actin polymerization
55 downstream of membrane signaling to drive various neuronal activities, including growth cone
56 formation, axon branching, dendrite branching, synapse formation, and axon guidance and
57 projection (Pilpel and Segal, 2005; Racz and Weinberg, 2008; Yamazaki et al., 2005). Disrupting
58 WRC in animals profoundly impacts the nervous system, leading to altered spine morphology
59 and density, intellectual disability, as well as embryonic lethality (Dahl et al., 2003; Soderling et
60 al., 2003). Mutations in WAVE and other subunits of the WRC lead to a variety of
61 neurodevelopmental disorders in human patients, including neurodevelopmental disorder with
62 absent language and variable seizures (NEDALVS), developmental and epileptic
63 encephalopathy-65 (DEE-65), and Alzheimer's disease (Begemann et al., 2021; Conway et al.,
64 2018; Ito et al., 2018; Kirkpatrick et al., 2017; Kumar et al., 2013; Olive et al., 2020; Shimojima
65 Yamamoto et al., 2021; Sims et al., 2017; Srivastava et al., 2021; Zhao et al., 2021; Zweier et al.,
66 2019).

67 WRC keeps WAVE basally inhibited by sequestering its C-terminal WCA to a conserved
68 surface formed by both the Sra1 and WAVE subunits (Chen et al., 2017a, 2010a; Eden et al.,
69 2002) . Through direct interactions, various molecules can recruit the WRC to the membrane
70 and/or simultaneously activate it, which releases the WCA to promote Arp2/3-mediated actin
71 polymerization. These ligands include small GTPases (e.g., Rac1 and Arf), acidic phospholipids
72 (e.g., PIP_3), various adaptor proteins, and over 100 different membrane proteins that contain a 6-

amino-acid peptide motif named the WIRS motif (WRC interacting receptor sequence, defined as Φ-x-T/S-F-x-x, where Φ is a bulky hydrophobic residue and x is any residues) (Chen et al., 2014a, 2017b, 2010a; Eden et al., 2002; Kobayashi et al., 1998; Koronakis et al., 2011; Lebensohn and Kirschner, 2009; Rottner et al., 2021). Many WIRS-containing membrane proteins, including Robo, Neogenin, Syg-1, neuroligins, and protocadherins, are important neuronal receptors and have been shown to rely on the WIRS-WRC interaction to regulate various processes in neural development (Chaudhari et al., 2021; Chia et al., 2014; Fan et al., 2018; Lee et al., 2016; Xing et al., 2018).

Previous studies identified the claudin-like dendrite receptor HPO-30 as a novel WRC binding protein, and this interaction was essential to higher-order dendrite branching. HPO-30 acts as co-receptor of the cell adhesion molecule DMA-1 in the PVD sensory neuron in C. elegans. The extracellular domains of HPO30 and DMA-1 form a multi-ligand complex with the secreted protein LECT2 and the extracellular domains of the epidermis cell receptors SAX7 and MNR1. These interactions provide the spatial cue for initiating dendrite branching (Dong et al., 2013; Zou et al., 2018, 2016). The intracellular domain (ICD) of HPO-30 directly binds the WRC, while the ICD of DMA-1 binds the guanine nucleotide exchange factor (GEF) TIAM-1, which can increase the local concentration of activated Rac1—the canonical activator of WRC. Together, HPO-30 and DMA-1 organize a multi-protein complex to spatiotemporally coordinate extracellular cues with the intracellular actin remodeling essential to high-order dendrite branching (Zou et al., 2018).

It is unclear how the HPO-30 ICD interacts with the WRC. It is also unknown if, in addition to binding WRC, the HPO-30 ICD has other functions. The HPO-30 ICD does not contain a WIRS motif and must use a non-WIRS mechanism to interact with the WRC. Previous

96 studies showed that deleting the C-terminal part of the HPO-30 ICD strongly affected WRC
97 binding *in vitro* and high-order dendrite branching *in vivo*, but it was unclear whether the HPO-
98 30 ICD used a linear peptide motif like WIRS to bind the WRC. Furthermore, the HPO-30 ICD
99 sequence is only conserved in nematode worms, but it binds to both *C. elegans* and human
100 WRC, suggesting that the interaction mechanism is conserved in other animals (Zou et al., 2018).
101 It is likely that humans have an unidentified membrane protein that uses the same interaction
102 surface to regulate the WRC. Thus, it is important to understand the mechanism underlying the
103 interaction between HPO-30 and the WRC.

104 Here we report biochemical and structural analysis of the HPO-30-WRC interaction. We
105 find that, unlike other WRC-interacting receptors known to date, HPO-30 is largely unstructured
106 in solution, but requires dimerization and folding into a three-dimensional structure to bind the
107 WRC. Furthermore, to our surprise, we find the HPO-30 ICD directly interacts with actin
108 filaments, also in a dimerization-dependent manner. This interaction potently inhibits both actin
109 polymerization and depolymerization. The dual activities of HPO-30 ICD provide an exciting
110 example of how a membrane receptor can modulate actin dynamics by simultaneously
111 controlling the localization of an actin nucleation factor and stabilizing local actin networks to
112 promote an important biological process.

113

114 **Results**

115 **HPO-30 ICD may use a folded structure, instead of a short peptide motif, to bind the WRC**

116 The HPO-30 ICD (or ICD for short hereafter) does not contain a WIRS motif. Therefore,
117 we first hypothesized it might use a distinct linear motif to bind the WRC. To identify this
118 sequence motif, we mutated every five residues to alanine throughout the ICD and used GST

119 pull-down assays to evaluate how they disrupted WRC binding (**Figure 1A**). To our surprise, we
120 found that mutating nearly any five amino acids (a.a.), except the last 6 a.a., significantly
121 reduced the binding to the WRC, with the middle region of the ICD showing the strongest effect
122 (**Figure 1A-C**, lanes 6-8). Interestingly, none of these 5-a.a. mutations completely abolished the
123 binding. This is consistent with our quantitative measurement of the binding affinity using
124 equilibrium pull-down assays, in which the wild type (WT) ICD had a dissociation constant (K_D)
125 of ~1.69 μM, while alanine mutant #5, which had the strongest effect in the non-equilibrium
126 pull-down assays (**Figure 1A,B,** lane 6), increased the K_D to ~5.06 μM (**Figure 1E, F**), still
127 maintaining significant binding (Kuzmic, 1996; Pollard, 2010). By contrast, deleting either the
128 entire N-terminal or C-terminal sequences, or combining two consecutive 5-a.a. mutations
129 almost completely abolished the binding (**Figure 1A** #11-14; **Figure 1D**). Note that while most
130 mutants contain a GST-tag at the N-terminus, the 5-a.a. mutations located at the C-terminus of
131 the ICD contain a GST-tag at the C-terminus (#8-#10 in **Figure 1**, lanes 9-11 in **Figure 1B**),
132 which we found protected the mutant ICDs from degradation (data not shown).

133 Nearly all of the 5-a.a. alanine scan mutants affected WRC binding, distinct from WIRS-
134 containing proteins where only mutations on the WIRS motif disrupted binding (Chen et al.,
135 2014b). We hypothesized that, instead of using a linear peptide motif, the HPO-30 ICD might
136 fold into a three-dimensional structure and use the folded structure to bind the WRC. Both
137 secondary structure analysis and various tertiary structure prediction programs unanimously
138 supported this hypothesis. For example, the recently published AlphaFold 2.0 and RoseTTA
139 Fold structural prediction software predicts the ICD contains alpha helical structure that overlaps
140 well with our binding data (**Figure 1G)** (Jumper et al., 2021; Minkyung et al., 2021). The above

141 mutagenesis and structural analysis suggest that HPO-30 ICD likely uses a folded tertiary
142 structure, instead of a linear peptide motif, to bind to WRC.

143 **HPO-30 ICD is unstructured in solution**

144 We tried several approaches to determine the structure of the HPO-30 ICD in isolation.
145 The ICD did not grow crystals by itself, when attached to solubility tags, or as a co-crystal with
146 the WRC. Nevertheless, due to its small size and our improved protocol to purify the isotope-
147 labeled ICD in high concentration, we were able to use nuclear magnetic resonance (NMR) to
148 obtain well-resolved ^{1}H-^{15}N HSQC spectra of untagged ^{15}N-labeled ICD (**Figure 2A**). From the
149 spectra of the untagged ICD, we can readily identify 50 distinct amide crosspeaks out of the 51
150 a.a. we predict to observe. The narrow ^{1}H chemical shift dispersion suggest that the HPO-30 is
151 predominantly disordered in solution. To further increase the stability and yield of untagged
152 ICD, we switched to using GB1-ICD, in which GB1 is a monomeric, small soluble tag
153 commonly used in NMR (Zhou and Wagner, 2010). Comparison of the 2D ^{1}H-^{15}N TROSY-
154 HSQC spectra collected for GB1-HPO-30 with the isolated HPO-30 **(Figure 2B)**, and with the
155 isolated GB1 **(Figure 2C),** show no significant chemical shift changes. This suggests that HPO-
156 30 remains largely disordered even when it is linked to a well-folded protein, such as GB1.
157 Furthermore, the NMR spectra were nearly identical at different protein concentrations (50 – 700
158 μM) and different temperatures (283 K – 298 K), suggesting the ICD alone does not undergo
159 structural changes in a concentration-dependent manner (data not shown).

160 This result is consistent with the circular dichroism (CD) spectrum of the ICD, in which
161 no major peak at either the beta-sheet wavelength (217nm) or the alpha-helix wavelengths (207
162 or 222nm) was observed, in contrast to the characteristic alpha-helical spectrum of BSA obtained

163 in the same conditions (**Figure 2E**). Together, these data suggest the purified ICD is unstructured
164 in solution.

165 **Dimerization is required for HPO-30 ICD to bind WRC**

166 Why does HPO-30 ICD lack secondary structure in solution, while seem to use a folded
167 structure to bind the WRC? In solving this conundrum, we realized that the GST-tagged
168 constructs used in our pull-down assays would dimerize the ICD, as GST is a constitutive dimer.
169 We then hypothesized that HPO-30 ICD may need to be dimerized for efficient binding to the
170 WRC. To test this hypothesis, we repeated the pull-down assay by switching the GST tag to a
171 monomeric tag, MBP (maltose binding protein). Consistent with our hypothesis, the MBP-tagged
172 ICD indeed showed very weak binding to the WRC (**Figure 3A**). Further supporting the
173 observation that monomeric ICD does not bind to WRC effectively, GST-ICD binding could not
174 be competed off by a chemically synthesized peptide covering the whole HPO-30 ICD, even
175 when the peptide was added in 5000-fold excess (**Supplemental Figure 1A**).

176 We next tested several different strategies to further validate if dimerization of the ICD is
177 required for WRC binding. First, we immobilized the WRC to the affinity beads by tethering a
178 dual MBP tag, $(MBP)_2$, to the WRC to pull down different monomeric vs. dimeric forms of
179 HPO-30 ICD. To our surprise, the WRC containing a $(MBP)_2$ tag at the N-terminus of HSPC300,
180 which was previously used to immobilize the WRC and pull down WIRS-containing proteins,
181 diminished HPO-30 ICD binding (Chen et al., 2014a). Similarly, the $(MBP)_2$ tag at the N-
182 terminus of Abi2 also prevented HPO-30 ICD binding (**Supplemental Figure 1B, C**). These
183 data suggest tagging $(MBP)_2$ at the N-terminus of HSPC300 or Abi2 may occlude the HPO-30
184 ICD binding surface (but not the WIRS binding surface). Finally, we were able to use sortase-
185 mediated protein ligation to tether a $(MBP)_2$ tag to the C-terminus of Abi2, which produced a

186 WRC that efficiently bound to amylose beads and effectively retained HPO-30 ICD
187 **(Supplemental Figure 1C, D)** (Chen et al., 2011). Using this construct, we observed robust
188 binding of all dimeric constructs we tested, including GST-ICD, ICD-GST, and DLC8-ICD
189 (DLC8 is a constitutive dimer from the dynein light chain) (Wang et al., 2003). By contrast, all
190 monomeric constructs, including GB1-ICD, sumo-ICD, and mEGFP-ICD showed very weak, if
191 any, binding (**Figure 3A**).

192 To further exclude the possibility that the affinity tags nonspecifically affected protein
193 interaction, we introduced the chemically inducible dimerizing (CID) tag FKBP and FRB to the
194 ICD, with the GB1 tag at the N-terminus to improve protein expression (Banaszynski et al.,
195 2005) (**Figure 3C**). In the presence of the dimerizer rapamycin, GB1-FKBP-ICD and GB1-FRB-
196 ICD can readily form a tight heterodimer, as confirmed by the gel filtration chromatography in
197 the presence and absence of rapamycin (**Supplemental Figure 1F**). Consistent with results from
198 the above constitutive dimeric tags, the addition of rapamycin significantly enhanced HPO-30
199 ICD binding (**Figure 3B**, right, lanes 8 and 9).

200 To ensure that the ICDs that contain different dimerization tags bind to the WRC using
201 the same mechanism, and to identify the optimal binding construct, we used competition pull-
202 down assays to compare different dimeric constructs. We found GST-ICD effectively competed
203 off both GB1-FKBP/FRB-ICD and DLC8-ICD binding to the WRC in a dose-dependent manner
204 (**Figure 3D**, left, lanes 4-6 and 8-10). The competition is specific, as the DLC8 tag by itself did
205 not bind to the WRC (**Supplemental Fig 1E**). Additionally, GB1-FKBP/FRB-ICD effectively
206 competed off GST-ICD binding to WRC only in the presence of rapamycin, while in the absence
207 of rapamycin, the competition efficiency was significantly reduced (**Figure 3D**, right, lanes 2-5).

208 These data further corroborate the notion that dimerized ICD promotes WRC binding, and that
209 all dimeric constructs tested so far bind WRC using the same mechanism.

210 As an alternative way to validate that dimerization of the HPO-30 ICD is required for
211 WRC binding, we mixed different GB1-FKBP/FRB constructs to produce various heterodimers
212 of the ICD. We found that having one ICD in the heterodimer (by mixing with empty GB1-
213 FKBP or FRB tag) or having a heterodimer of WT ICD with the alanine #5 mutant ICD failed to
214 support robust binding to the WRC, compared to the dimer containing both WT ICDs in the
215 same total concentration of the WT ICD (**Figure 3E, F**; lanes 3, 5, and 6 are WT dimer and
216 heterodimer, respectively). Taken together, our data suggest that dimerization of two functional
217 HPO-30 ICD moieties are required for efficient binding to the WRC.

218 **Dimerization is not sufficient to induce HPO-30 ICD folding**

219 As the dimerized ICD binds to the WRC more potently than monomeric proteins, we
220 tested if dimerization could induce structure changes in the HPO-30 ICD. For this experiment,
221 we could not obtain dimerized ICDs in high enough concentration except for GST-ICD. With
222 this material, we obtained 2D NMR spectra, which showed ^{1}H chemical shift dispersion nearly
223 identical to the untagged ICD, indicating that dimerization alone is not enough to induce
224 significant ICD folding (**Figure 2D**). Based on the above evidence, we posit that the HPO-30
225 ICD needs to undergo both dimerization and induced folding in order to bind to the WRC. High-
226 resolution structural information will be necessary to confirm this hypothesis. This induced
227 folding has been proposed for many DNA-binding proteins and some cell-signaling molecules
228 (Dyson and Wright, 2002; Turjanski et al., 2008). Interestingly, the structure predictions for
229 dimeric protein match the structure predicted for monomeric protein and corroborate our
230 mutagenesis data **(Supplemental Figure 1G)**.

231 **HPO-30 ICD inhibits both actin polymerization and depolymerization**

232 Previously studies have shown that Rac1 is a canonical activator of the WRC, and
233 various WIRS-containing receptors could further fine tune WRC activity, likely through
234 secondary weak interactions between the sequence flanking the WIRS motif and the WRC (Chen
235 et al., 2014a). After establishing that dimeric ICD robustly binds the WRC, we tested if the
236 interaction could similarly influence WRC activity in promoting Arp2/3-mediated actin
237 polymerization. (Cooper et al., 1983; Doolittle et al., 2013a; Kouyama and Mihashi, 1981).
238 While optimizing the pyrene-actin polymerization assay, we noticed that buffer conditions have
239 a significant impact on the ICD-WRC interaction. The commonly used pyrene-actin assay buffer,
240 50KMEI20Gd (50mM KCl, 2mM $MgCl_2$, 1mM EGTA pH 8.0, 10mM Imidazole pH 7.0, 20%
241 (w/v) glycerol, 1mM DTT), reduced WRC binding, while lowering the concentration of glycerol
242 to 5% and replacing imidazole with HEPES at the same pH rescued binding (**Supplemental**
243 **Figure 2A**). Using this optimized buffer (50KMEH5Gd), we tested the effect of monomeric and
244 dimeric HPO-30 ICD using our inducible dimerization constructs (**Figure 3C**). We observed that
245 HPO-30 caused a dimer- and concentration-dependent decrease in WRC-mediated actin
246 polymerization (**Figure 4A**). Dimeric HPO-30 was more effective at reducing actin
247 polymerization from Rac1-mediated WRC activity, although both monomeric and dimeric HPO-
248 30 reduced polymerization to the same level at the highest concentration tested (**Figure 4A**).
249 Rapamycin alone had no effect on actin polymerization mediated by the WRC (**Supplemental**
250 **Figure 4B**). This effect was not based on inhibition of the WRC, as HPO-30 could inhibit actin
251 polymerization mediated by free WCA as well as basal activity of actin and Arp2/3 alone
252 (**Figure 4B, C**).

253 We wondered if the WRC-independent inhibitory effect of HPO-30 ICD was due to the
254 ICD binding to and sequestering free G-actin. However, we observed no obvious binding
255 between GST-HPO-30 and actin or GB1-FKBP-HPO-30/GB1-FRB-HPO-30 and actin
256 (**Supplemental Figure 2C, D**). This suggests the ICD may inhibit actin polymerization by
257 binding to filamentous, rather than the monomeric, actin. We then used actin filament pelleting
258 assays to measure ICD binding to polymerized actin (Heier et al., 2017) (**Figure 4D**). We found
259 that significantly more dimerized HPO-30 (30.4% ± 4.3%) was pelleted with actin, compared to
260 BSA (0.7% ± 0.7%), dimeric empty vector (9.3% ± 2.6%), and the F-actin barbed end binding
261 protein, CapZ (7.6% ± 3.3%). Surprisingly, significantly more monomeric HPO-30 (22.1% ±
262 4.2%) was also pelleted than BSA and monomeric empty vector (2.3% ± 1.6%) (**Figure 4E**).
263 This suggests that monomeric ICD, while not as effective in inhibiting actin polymerization as
264 the dimeric ICD, is also capable of binding to actin filaments. Together, these data led us to a
265 hypothesis that HPO-30 ICD may bind to actin filaments to prevent actin polymerization.
266 Proteins that can potently inhibit actin polymerization are called capping proteins (e.g.,
267 CapZ), which bind to the barbed end of actin filaments to inhibit filament growth (Caldwell et
268 al., 1989; Weeds and Maciver, 1993). To test if HPO-30 may act as a capping protein, we used a
269 depolymerization assay that has been used to measure CapZ activity previously (**Figure 4F** for
270 example curves, **Figure 4G** for quantification) (Caldwell et al., 1989). We found that, similar to
271 CapZ, HPO-30 prevented actin depolymerization (**Figure 4F, G**) (Caldwell et al., 1989; Cooper
272 and Pollard, 1985). Interestingly, this activity was both concentration- and dimerization-
273 dependent, similar to the effect in promoting WRC binding, suggesting dimerization and perhaps
274 induced folding are also involved in this capping-like activity. Unfortunately, this strong

275 inhibitory effect on actin polymerization and depolymerization prevented us from directly
276 measuring the effect of HPO-30 ICD on WRC activation.

277 **HPO-30 ICD binds to actin filaments**

278 The above bulk solution assays suggest HPO-30 ICD may act as a capping protein to
279 inhibit both polymerization and depolymerization. To directly validate this activity, we used
280 single-molecule total internal reflection fluorescence (smTIRF) microscopy to visualize where
281 HPO-30 ICD binds to actin filaments. To properly label proteins with fluorophores, we fused a
282 SNAP tag to the N-terminus of the CapZ beta-subunit, FKBP-HPO-30, FRB-HPO-30, FKBP,
283 and FRB. The SNAP-tagged HPO-30 proteins were capable of binding the WRC in a rapamycin-
284 dependent manner and to a similar level as the GB1 proteins, suggesting SNAP-tag did not affect
285 HPO-30 binding to the WRC (**Supplemental Figure 3A**, middle, lanes 2 and 4). SNAP-CapZ,
286 SNAP-FKBP, and SNAP-FKBP-HPO-30 were labeled using SNAP-Surface® AlexaFluor® dyes
287 (**Supplemental Figure 3B**). After being labeled, all CapZ proteins and SNAP-Surface®
288 AlexaFluor®-488 and SNAP-Surface® AlexaFluor®-546 labeled HPO-30 ICD exhibit similar
289 capping activity as the previous constructs in our bulk solution assay (**Supplemental Figure**
290 **3C**). Hereafter, labeled proteins will be referred to as the protein name followed by the dye
291 excitation wavelength (e.g., SNAP-CapZ-488 for SNAP-CapZ labeled with SNAP-Surface®
292 AlexaFluor®-488).

293 In the smTIRF experiments, at low protein concentrations (5 nM) we could observe
294 SNAP-CapZ-488 bound to the barbed end of filaments, where it moved with filaments and
295 stopped their growth (**Figure 5A**, top). Note that in this time-lapse the filament and CapZ-488
296 puncta are displaced at 79.52s (marked by a white arrow), but align again at 80.02s. This is due
297 to the image acquisition condition—to prevent photobleaching, images in the 640 nm-channel

298 were taken every 20 acquisitions of the 547 nm-channel. By comparison, when we used 15 nM
299 SNAP-FKBP-ICD-546/15 nM SNAP-FRB-HPO-30 (and 8-fold molar excess of rapamycin), we
300 observed binding between HPO-30 ICD and actin filaments, but none seemed to cap the
301 filaments as we saw for CapZ. In the bottom panel of **Figure 5A**, HPO-30 binds near the barbed
302 end of the filament (time 36.54s), after which the filament continues to polymerize while the
303 HPO-30 ICD molecule stays bound to the same position. At 200.02s, the puncta moves away
304 from the filament, followed by the filament moving to the same spot at 200.57s (marked by a
305 white arrow)—again a lag of colocalization caused by the imaging condition.

306 We quantified all binding events using stringent criteria to prevent misidentification of
307 background signal as a binding event (see Materials and Methods) and found that 33% of
308 filaments had at least one binding event over the course of the 15-minute duration of the
309 experiment. This was significantly higher than the number of events seen using identical
310 conditions and labeled empty vector (**Figure 5B**, left). We binned the filaments based on how
311 many contained 0 events, 1 event, and 2 events and compared HPO-30 and empty vector (**Figure**
312 **5B**, right). Due to the high background and lower affinity of HPO-30 than CapZ, we were not
313 able to use high concentrations of HPO-30 ICD to observe robust capping events; furthermore,
314 the side-binding activity also makes it difficult to distinguish if any capping events that we see
315 are coincidental with side binding due to light diffraction limit. Together with the F-actin
316 pelleting assay results, these data suggest that HPO-30 possesses the ability to bind actin
317 filaments in a manner different from CapZ, but resulting in inhibiting actin polymerization and
318 depolymerization similar to CapZ (**Figure D, E**).

319 To directly observe the effect of HPO-30 ICD on actin filament growth, we used 1μM
320 unlabeled SNAP-FKBP-HPO-30/SNAP-FRB-HPO-30 (with 8-fold molar excess of rapamycin)

321 and quantified the growth rate of individual actin filaments (Kuhn and Pollard, 2005) (**Figure**
322 **5C**). The addition of dimeric ICD significantly slowed actin elongation rate (1.511 ± 0.272
323 subunits/second) compared to actin alone (2.28 ± 0.48 subunits/second) (**Figure 5C**). Addition
324 of monomeric ICD also significantly slowed down actin elongation rate (1.99 ± 0.41
325 subunits/second) compared to actin alone, suggesting that the side-binding activity of the ICD
326 may be capable of slowing down actin polymerization. Importantly, empty SNAP vector protein
327 had no effect on the actin polymerization rate (2.13 ± 0.42 subunits/second). Very low amounts
328 of CapZ (5 nM) were able to decrease the rate to significantly lower than dimeric HPO-30 (0.30
329 ± 0.13 subunits/second), confirming again that CapZ and HPO-30 ICD likely achieve the same
330 effect on actin dynamics by using different mechanisms. Taken together, our data supports our
331 hypothesis that HPO-30 is capable of inhibiting actin polymerization and depolymerization.
332

333 **Discussion**

334 HPO-30 is required for higher order dendrite branching in C. elegans PVD neurons, a
335 function that requires its ability to bind to the WRC (Zou et al., 2018). The WRC, as an Arp2/3
336 activator, generates branched actin networks that can deform the membrane, serving to localize
337 actin polymerization and generate new branches at where HPO-30 is enriched. However, the
338 mechanism by which HPO-30 and the WRC control dendrite branching were not known. Here,
339 we show that the HPO-30 ICD likely uses a folded domain to bind to the WRC, rather than the
340 short WIRS motif found in many other neuronal receptors (**Figure 1**), even though the isolated
341 HPO-30 ICD is likely unstructured by itself (**Figure 2**) (Chen et al., 2014a). We also
342 demonstrate that HPO-30 binding requires dimerization, but dimerization alone is not enough to
343 induce structure, which suggests that binding to the WRC induces folding in the HPO-30 ICD

344 (**Figures 2, 3**). Remarkably, while attempting to characterize the effect HPO-30 of on WRC
345 activity, we discovered that HPO-30 ICD can bind to actin filaments and act to modulate both
346 polymerization and depolymerization. Thus, the HPO-30 ICD possesses two distinct actin
347 regulatory mechanisms, which would provide exquisite fine tuning of local actin dynamics
348 (**Figure 6**, and see discussion below).

349 While our data suggests HPO-30 is unstructured by itself, we posit that structure could be
350 induced by binding to the WRC (or other ligands) or by the oligomerization state of protein in
351 cells (Dyson and Wright, 2002) (**Figure 2**). This is supported by our biochemical data and
352 structural predictions, which identify regions of alpha-helical structure in the N-terminus of
353 HPO-30 that overlap well with regions that affect binding (Jumper et al., 2021) (**Figure 1**).
354 Whatever form it may take, this binding structure should be conserved, as the HPO-30 ICD is
355 conserved only in nematodes, but can bind to human WRC (Zou et al., 2018). HPO-30 then
356 represents a new class of transmembrane proteins that can interact with the WRC using a folded
357 domain, separate from the already identified WIRS receptors that use a linear motif to bind the
358 WRC (Chen et al., 2014a). Solving the high-resolution structure of the HPO-30 ICD bound to the
359 WRC would allow us to look for structural homologues of HPO-30 using both structure and
360 sequence of the binding residues as a guide and would allow us to identify the biological
361 process(es) this family plays an important role in. As WRC is too large for NMR and current
362 crystal conditions for the WRC do not support HPO-30 binding, cryo-EM will be ideal for
363 solving the structure of the HPO-30-WRC complex, especially as models for the WRC in the
364 inactive and Rac-bound state have been solved (Chen et al., 2017b, 2010a). As the HPO-30 ICD
365 is unstructured, it is possible that binding to actin filaments causes HPO-30 to adopt a different

366 conformation than binding to the WRC does. Similarly, high-resolution structure of the HPO-30
367 ICD bound to actin filaments would allow for identification of the interaction mechanism.
368 We also show that binding between HPO-30 and the WRC is greatly enhanced by
369 dimerization of the HPO-30 ICD (**Figure** 3). Dimerization enhanced binding of HPO-30 would
370 provide a mechanism of regulation for the HPO-30-WRC interaction. Dimerization of the FL
371 HPO-30 could be induced by increased protein concentration at sites of protrusion or specific
372 signaling events that cause clustering of the HPO-30 receptors. HPO-30 is known to form a large
373 signaling complex with DMA-1 from PVD neurons, MNR-1 and SAX-7 from epidermal cells,
374 and the secreted protein LECT-2 (Zou et al., 2018). Investigating what effect this signaling
375 complex has on the local concentration or the oligomerization state of HPO-30 would provide a
376 mechanism of how cells can control HPO-30 dimerization and subsequent WRC binding.
377 The effect of HPO-30 on the ability of the WRC to polymerize actin was confounded by
378 its strong inhibition of actin polymerization (**Figure 4A, B, C**). We speculate that HPO-30 may
379 not activate the WRC and serves only to localize it to the dendrite branching sites, but we cannot
380 rule out the possibility of the ICD influencing WRC activation. Using an actin independent
381 method to assess WRC activation, such as a FRET-based sensor to monitor WCA release, would
382 allow us to identify any effect HPO-30 could have on the WRC. Such a method, however, is
383 currently unavailable.
384 The ability of HPO-30 to inhibit actin polymerization and depolymerization is exciting.
385 To our knowledge, this represents the first transmembrane protein capable of direct interaction
386 with both an actin nucleation promotion factor and actin. Unfortunately, the affinity between
387 HPO-30 and actin was too low for us to visualize HPO-30 capping actin filaments using single
388 molecule assays (**Figure 5A**). If HPO-30 has a lower affinity towards the barbed ends than actin

389 monomers, this could explain the differences we see between polymerization and
390 depolymerization experiments—HPO-30 functions as a capping protein at lower concentrations
391 in depolymerization experiments because it does not have to compete for binding to the barbed
392 end with actin monomers. Because we cannot rule out that HPO-30 possesses both capping and
393 side-binding activity, we propose that HPO-30 possesses a "gating" ability, based on the
394 preference for side-binding near the barbed end and the reduction in polymerization speed
395 (**Figure 5**). Our data reveal that monomeric HPO-30 is still capable of binding to actin filaments
396 but is weaker towards inhibiting polymerization and depolymerization than the dimeric form.
397 This could be due to a simple difference in affinity between monomeric and dimeric HPO-30 and
398 the actin filaments. However, we do not see a significant difference in the amount of HPO-30
399 that is pelleted with F-actin between monomeric and dimeric protein, suggesting they have
400 similar affinities (**Figure 4D, E**). This gives rise to an attractive model in which monomeric and
401 dimeric HPO-30 are both capable of binding to the sides of filaments, but dimeric HPO-30 is
402 capable of capping or "gating" filaments by binding to the barbed end. This proposed mechanism
403 is similar to how tropomyosin and tropomodulin function, in which tropomyosin coats filaments
404 and stabilizes them against ADF/cofilin depolymerization, while tropomodulin "caps" the
405 tropomyosin (Mudry et al., 2003).

406 The abilities to localize the WRC to the membrane (which promotes Arp2/3-mediated
407 actin polymerization) and to simultaneously slow down actin polymerization seem to be
408 conflicting functions. However, CapZ has been found to be essential for actin- and Arp2/3-based
409 motility in both *in vitro* bead motility assays and *in vivo* processes (Akin and Mullins, 2008;
410 Miyoshi et al., 2006). The proposed mechanism is that CapZ, by blocking actin from barbed
411 ends, stimulates the formation of new branches through Arp2/3, thereby changing the actin

412 architecture such that more force is generated against the surface the actin is localized to (Akin
413 and Mullins, 2008). In a similar manner, HPO-30 is capable of stimulating actin polymerization
414 mediated by the WRC and Arp2/3 when present in a state which weakly binds actin – namely, in
415 low concentration and a monomeric form. In **Figure 4A**, 1 μM HPO-30 ICD with DMSO
416 potently enhances actin polymerization above just WRC and Rac alone.

417 Together, our data lead to an exciting model (**Figure 6**). HPO-30 dimerization promotes
418 binding to the WRC, which induces folding of the ICD. This binding will localize the WRC to
419 branching sites within the PVD neuron to initiate WRC-Arp2/3 mediated actin polymerization
420 (**Figure 6**, top left). Importantly, HPO-30 co-localizes with DMA-1, which can interact with the
421 Rac-GEF Tiam1 and would serve to keep the WRC activated, irrespective of whether HPO-30
422 ICD itself has a stimulatory effect on WRC activity (Zou et al., 2018). At the same time, HPO-30
423 can bind to the sides of actin filaments in the monomeric and dimeric form to slow down
424 polymerization/depolymerization, either by side binding or capping activities (**Figure 6**, top
425 right). Note that we do not know if the ICD uses a structure to bind to actin as it does to the
426 WRC. Further work will be required to determine how HPO-30 interacts with filaments. HPO-
427 30, by binding to actin filaments and the WRC at the same locations on the membrane, would
428 promote the formation of more highly branched actin networks, likely in a manner analogous to
429 CapZ (**Figure 6**, bottom). This dual actin binding ability could be one mechanism by which the
430 swellings at branch points observed in PVD neurons are formed (Shi et al., 2021). Further
431 investigation into how the HPO-30 ICD binds to both the WRC and actin will potentially reveal
432 a new class of proteins that can regulate multiple steps of the actin polymerization process,
433 allowing for greater control of local actin dynamics.
434

435 **Methods and Materials**

436 ***Protein Expression and Purification***

437 GST-HPO-30 and associated alanine mutants, HPO-30-GST and associated alanine
438 mutants, DLC8-HPO-30-His6, GB1-HPO-30-His6, His9-sumo-HPO-30, MBP-HPO-30-mEGFP,
439 GB1-FKBP-HPO-30-His6 and associated alanine mutant, GB1-FRB-HPO-30-His6 and
440 associated alanine mutant, GB1-FKBP-His6, GB1-FRB-His6, SNAP-FKBP-HPO-30-His6,
441 SNAP-FRB-HPO-30-His6, SNAP-FKBP-His6, SNAP-FRB-His6, MBP-WAVE1 (1-230), MBP-
442 WAVE1 (1-230)-VCA, MBP-WAVE1 (1-178), MBP-Abi2 (1-158), MBP-HSPC300, 2MBP-
443 Abi2 (1-158), 2MBP-HSPC300, and Rac1 QP Δ4 were individually expressed in Arctic Express
444 (DE3) RIL (Agilent) or BL21 (DE3) $T1^R$ (Sigma) cells after induction with 0.75 mM IPTG at 10
445 °C or 18 °C for 16 hours. His10-SNAP-CapZ β and CapZ α expressed together from the pCDF
446 Duet vector in Arctic Express (DE3) RIL (Agilent) cells after induction with 0.75 mM IPTG at
447 10 °C for 16 hours. GST-HPO-30 and alanine mutants, HPO-30-GST and alanine mutants, and
448 GST-mEGFP were purified through Glutathione Sepharose beads (GE Healthcare), followed by
449 cation exchange chromatography using a Source 15S column (GE Healthcare) at pH 7.0. MBP-
450 HPO-30 was purified through amylose resin (New England Biolabs). The GST tag from GST-
451 HPO-30-mEGFP and the MBP tag from MBP-HPO-30 were removed using TEV cleavage at 4
452 °C overnight, followed by cation exchange chromatography using a Source 15S column (GE
453 Healthcare) at pH 7.0. DLC8-HPO-30-His6, GB1-HPO-30-His6, His9-sumo-HPO-30, GB1-
454 FKBP-HPO-30-His6 and associated alanine mutant, GB1-FRB-HPO-30-His6 and associated
455 alanine mutant, GB1-FKBP-His6, GB1-FRB-His6, SNAP-FKBP-HPO-30-His6, SNAP-FRB-
456 HPO-30-His6, SNAP-FKBP-His6, and SNAP-FRB-His6 were purified through Ni-NTA
457 Agarose resin (Qiagen), followed by cation exchange chromatography using a Source 15S

458 column (GE Healthcare) at pH 7.0. GST-HPO-30, HPO-30-GST, DLC8-HPO-30-His6, GB1-
459 HPO-30-His6, His6-sumo-HPO-30, HPO-30-mEGFP, untagged HPO-30, GB1-FKBP-HPO-30-
460 His6 and associated alanine mutant, GB1-FRB-HPO-30-His6 and associated alanine mutant,
461 GB1-FKBP-His6, GB1-FRB-His6, SNAP-FKBP-HPO-30-His6, SNAP-FRB-HPO-30-His6,
462 SNAP-FKBP-His6, SNAP-FRB-His6 were further purified through a Superdex 75 column (GE
463 Healthcare). His10-SNAP-CapZ β and CapZ α were purified through Ni-NTA Agarose resin
464 (Qiagen), followed by anion exchange chromatography using a Source 15Q column (GE
465 Healthcare) at pH 8.0 and size exclusion chromatography on a Superdex200 column (GE
466 Healthcare). Rac1 QP Δ4 was purified by an SP-Sepharose Fast Flow column (GE Healthcare) at
467 pH 7.0 followed by size exclusion chromatography through a Superdex 75 column.
468 MBP-WAVE1, MBP-Abi2, MBP-HSPC300, 2MBP-Abi2, and 2MBP-HSPC300 proteins
469 were purified through amylose beads (New England Biolabs). His6-Sra1 and Nap1 dimer were
470 co-expressed in Tni insect cells (Expression systems), and the dimer was purified through Ni-
471 NTA agarose resin (Qiagen) followed by anion exchange chromatography using a Source 15Q
472 column at pH 8.0. Pentameric WRC was assembled and purified by following previously
473 described protocols (Chen et al., 2014c, 2010b). Briefly, individually purified WAVE1, Abi2,
474 and HSPC300 subunits were mixed at equimolar ratio in the presence of 1% (w/v) NP40 and
475 incubated on ice for 48 hours. The assembled trimer was then purified by anion exchange
476 chromatography through a Source 15Q column at pH 8.0, cation exchange chromatography by a
477 Source 15S column at pH 6.0, and size exclusion chromatography through a Superdex 200
478 column (GE Healthcare). Dimer and trimer were mixer at equimolar ratio and incubated on ice
479 for 30 min. The assembled pentamer was purified on amylose beads (NEB) and the MBP and
480 His6 tags were cleaved using TEV protease incubation overnight. The pentamer was further

481 purified using anion exchange chromatography through a Source 15Q column at pH 8.0 and size
482 exclusion chromatography using a Superdex 200 column.

483 Actin was purified as previously described from rabbit muscle acetone powder from Pel-
484 Freeze (Spudich and Watt, 1971). Actin was pyrene labeled or Alexa Fluor® 647 labeled after
485 polymerization at 4 °C, using a 10-fold or 2-fold excess dye, respectively. Actin and pyrene actin
486 for actin polymerization and depolymerization assays were kept in continuous dialysis at 4 °C,
487 with biweekly buffer changes. Actin and Alexa Fluor® 647-labeled actin for smTIRF
488 experiments were kept in closed tubes for two weeks.

489 ***WRC-(MBP)$_2$ Generation***

490 To create WRC-(MBP)$_2$, MBP-Abi2 (1-158) had LPGTG genetically fused to the C-
491 terminus and a TEV site was added to the N-terminus of the 2MBP tag to generate a Gly after
492 cleavage. MBP-Abi2 (1-158)-LPGTG was expressed, purified, and incorporated into the WRC
493 as above to create WRC-LPGTG. GG-2MBP was expressed in Arctic Express (DE3) RIL
494 (Agilent) cells after induction with 0.75 mM IPTG at 10 °C for 16 hours, purified on amylose
495 resin, and subjected to TEV cleavage overnight, followed by anion exchange chromatography
496 using a SourceQ15 column (GE Healthcare). Sortase5M (sortase A pentamutant) was a gift from
497 David Liu (Addgene plasmid # 75144), expressed in Arctic Express (DE3) RIL (Agilent) cells,
498 purified over Ni-NTA agarose resin, followed by cation exchange using a Source 15S column
499 (GE Healthcare) and size exclusion chromatography using a Superdex 75 column (GE
500 Healthcare) (Chen et al., 2011). 1 μM WRC-LPGTG was mixed with 25 μM GG-MBP and 10
501 μM sortase in 50 mM Tris pH 7.5, 150 mM NaCl, and 10 mM $CaCl_2$ and left at room
502 temperature for two hours. The reaction was quenched by adding 25 mM EGTA and the WRC-

503 $(MBP)_2$ was purified over a Superdex 200 column to separate the WRC-$(MBP)_2$ from unligated
504 products.

505 ***Protein Pull-Down Assays***

506 GST pull-down assays were performed as previously described (Shi et al., 2021). Briefly,
507 20 µL of GSH-Sepharose beads were mixed with bait protein and prey protein in 1 mL of pull-
508 down buffer (50 mM NaCl, 10 mM HEPES pH 7.0, 5% (w/v) glycerol, 5 mM 2-
509 mercaptoethanol, and 0.05% Triton X-100). The samples were mixed at 4 °C for 30 minutes,
510 washed three times with 1 mL of pull-down buffer, and eluted with 40 µL of elution buffer
511 containing 30 mM reduced glutathione and 100 mM Tris pH 8.5. The eluant was examined by
512 SDS-PAGE and Coomassie blue staining. MBP pull-down assays were performed like GST pull-
513 down assays, instead using 20 uL of amylose resin and elution buffer (pull-down buffer
514 supplemented with 2% [w/v] maltose). The eluant was examined by SDS-PAGE and Coomassie
515 blue staining. His-tagged pull-down assays were performed as above, instead using 20 uL of Ni-
516 NTA agarose resin, G-Buffer as the wash buffer, and elution buffer containing 500 mM
517 imidazole pH 7.0. The eluant was examined by SDS-PAGE and Coomassie blue staining. In all
518 pull-down assays using FKBP and FRB, rapamycin was added to 5 µM final concentration. For
519 DMSO controls, the same volume DMSO was added instead. For the alanine scan pull-down
520 quantification, the intensity of the Sra1 and Nap1 bands were quantified using ImageJ. The
521 intensity from the GST control lane was subtracted from the alanine protein lane, and the
522 corrected intensity was divided by the intensity of the wild type HPO-30. A students paired t-test
523 was used to compare the wild type and each mutant separately.

524 ***Equilibrium Pulldown Assays***

525 Equilibrium pulldown assays were performed as previously described (Chen et al.,
526 2017b). Briefly, 60 uL of GSH-Sepharose beads were mixed with 0.1 μM WRC and various
527 amounts of GST-tagged protein (from 0.01 μM to 30 μM) and brought to 100 uL with pull down
528 buffer. The reactions were allowed to mix for 30 min at 4 °C, and four reactions at a time were
529 spun at 15 krpm for 15 seconds. The supernatant was removed and examined by SDS-PAGE and
530 Coomassie blue staining. Each assay was repeated 3 times. The Sra1/Nap1 intensity was
531 quantified using ImageJ and the fractional occupancy was calculated. The data was fit using a
532 single binding site model using DynaFit (Kuzmic, 1996).

533 ***Gel Filtration Assays***

534 GB1-FKBP-HPO-30 and GB1-FRB-HPO-30 were mixed at equimolar ratio and run over
535 a Superdex 200 column (GE healthcare) in 100 mM NaCl, 10 mM HEPES pH 7.0, 5% (w/v)
536 glycerol, and 1 mM DTT with or without rapamycin.

537 ***Actin Polymerization Assays***

538 Actin polymerization assays, or activity assays, were performed as previously described
539 (Doolittle et al., 2013a). Actin was purified and pyrene-labeled as described above and kept in
540 continuous dialysis in G-Buffer (2 mM Tris-HCl pH 8, 0.5 mM DTT, 0.2 mM ATP, 0.1 mM
541 $CaCl_2$, 1 mM NaN_3) that is changed twice a week. Arp2/3 was purified following existing
542 protocols and kept aliquoted at -80°C (Doolittle et al., 2013b). All proteins except for the WRC
543 and Arp2/3 were purified into 50KMEH5Gd (50 mM KCl, 1 mM $MgCl_2$, 1 mM EGTA, 10 mM
544 HEPES pH 7.0, 5% (w/v) glycerol, 1 mM DTT) and stored at -80°C. WRC230VCA was purified
545 into 100KMEI20Gd (100 mM KCl, 10mM Imidazole pH 7.0, 20% [w/v] glycerol) and kept at -
546 80°C. 4 μM actin with 5% pyrene labeled and 10 nM Arp2/3 were used for all assays. 100 nM
547 WRC230VCA or 100 nM free VCA was added to all reactions labeled "WRC." 0.4 μM Rac1

548 Q61L/P29S-Δ4 was used for all conditions labeled "Rac." 5 μM rapamycin was added where
549 indicated or an equivalent volume DMSO. The excitation and emission wavelengths were set to
550 365 nm and 407 nm, respectively. Data were collected on a TECAN SPARK plate reader.

551 ***Actin Depolymerization Assays***

552 Actin polymerization assays were performed as previously described, with some
553 modifications (Heiss and Cooper, 1991). Actin at ~20 μM and 70% pyrene-labeling was pre-
554 polymerized at room temperature overnight by addition of 1 mM $MgCl_2$ and 50 mM KCl. For
555 each reaction, actin was diluted to 5 μM in one mix, either alone or with protein, and left for 3
556 minutes at room temperature to allow for protein binding. Protein at the same concentration was
557 prepared in a separate mix and, after 3 minutes, the actin was further diluted 20-fold by the
558 addition of the second mix. The excitation and emission wavelengths were set to 365 nm and 407
559 nm, respectively. Data were collected on a TECAN SPARK plate reader. To calculate the
560 relative initial velocity, the slope for the first 30 seconds of the reaction was calculated and
561 divided by the slope of the actin control. ANOVA on Ranks and Dunn-Tukey tests were
562 performed to determine significance.

563 ***Circular Dichroism***

564 Untagged HPO-30 was purified into 100 mM NaCl, 10 mM HEPES pH 7.0, 5% (w/v)
565 glycerol, and 1 mM DTT. The same buffer was used to dissolve powdered BSA and as a blank
566 for the CD spectrometer. The blank buffer was degassed by sonication for 3 minutes at 30%
567 power. Data were collected on a MOS-500 fluorimeter using an ALX250 lamp. Data were
568 collected for wavelengths between 190 nm and 260 nm, with a 1 nm step, 0.5 s acquisition
569 period, and averaged over three repeats. Mean residue ellipticity was calculated as described
570 previously (Greenfield, 2006). Data for BSA and HPO-30 were collected at the same

571 concentration of protein. TMAO was dissolved to 3 M in the same buffer as HPO-30 purification
572 and was added to the appropriate concentration before measuring. New blanks for TMAO were
573 measured to ensure TMAO alone had no effect on the spectrum.

574 ***NMR***

575 Isotopically labeled proteins were expressed and purified as described for non-labeled
576 proteins, using minimal media containing N^{15} NH_4Cl instead of traditional media. Proteins were
577 purified into 100 mM NaCl, 10mM HEPES pH 7.0, 5% (w/v) glycerol, 1 mM DTT and were
578 supplemented with 10% D_2O. Proteins ranged in concentration from 70 µM (GB1 tag) to 850
579 µM (GB1-HPO-30). GB1 tag was produced by thrombin cleavage of GB1-HPO-30 and removal
580 of HPO-30 using nickel-NTA resin (Qiagen). NMR spectra were collected on a Bruker 700 MHz
581 spectrometer equipped with z-shielded gradient triple resonance 5 mm TCI cryoprobe. 2D 1H-
582 15N TROSY-HSQC experiments were recorded with a time domain matrix consisting of 100*
583 (t1, 15N) × 1024* (t2, 1H) complex points with acquisition time of 50 ms (t1) and 91.8 ms (t2)
584 using 16 scans per FID and 1.5 s interscan delay. Spectral widths for 1H and 15N dimensions
585 were set to 15.9 and 28.2 ppm, respectively, with carriers set at 4.821 ppm (1H) and 119.138
586 ppm (15N).

587 ***Protein Labeling***

588 SNAP-tagged proteins were labeled with SNAP-Surface® Alexa Fluor® 488, SNAP-
589 Surface® Alexa Fluor® 546, and SNAP-Surface® Alexa Fluor® 647 from New England Biolabs.
590 5 µM protein and 10 µM dye were mixed and allowed to react in 50KMEH5Gd at room
591 temperature for two hours, followed by desalting into 50KMEH5Gd buffer and concentration.
592 Dye extinction coefficients were calculated from a standard curve and are as follows: Alexa 488
593 at 495 nm, 95000 $M^{-1}*cm^{-1}$; Alexa 546 at 556 nm, 120000 $M^{-1}*cm^{-1}$; Alexa 647 at 650 nm,

594 255000 $M^{-1}*cm^{-1}$. Protein labeling efficiency was calculated by dividing protein concentration
595 by dye concentration– for Alexa Fluor® 488 the labeling efficiency was estimated at ~100%, for
596 Alexa Fluor® 546 the labeling efficiency was estimated at ~60%.

597 ***smTIRF Data Collection***

598 All videos were collected on a Nikon TE2000-E inverted microscope equipped with a
599 100x 1.49 NA TIRF objective and a TIRF Quad filter cube (Chroma C141789), using an Andor
600 iXon3 EM-CCD (DU-897-CS0) camera, with a GATACA iLas system to prevent uneven
601 illumination. Coverslips were prepared as described previously, with slight modifications
602 (Narvaez-Ortiz and Nolen, 2022). Briefly, glass coverslips were cleaned with 2% (w/v)
603 Hellmanex, acetone, and 1 M KOH solutions with sonication, rinsing heavily with DI water
604 before each step and after the KOH treatment. Coverslips were rinsed with methanol and dried
605 using a N_2 gas stream. GOPTES was added to the coverslips and baked at 75°C for 30 minutes.
606 Coverslips were rinsed with microscope grade ethanol and dried with N_2 gas stream. A 2% (w/w)
607 Biotin-PEG3000/NH2-PEG3000 mixture of powder was prepared, placed on top of the
608 coverslips, and the coverslips baked overnight at 75°C. After overnight baking, the coverslips
609 were washed with water and dried with N_2 gas. Individual wells were made by placing
610 functionalized coverslips on Ibidi® sticky-Slide IV 0.4 slides. Individual lanes were prepared for
611 microscopy by incubating with 5% (w/v) PF-127 for 10 min at RT, followed by either 100 nM
612 (for elongation rate analysis) or 35 nM (for side binding analysis) neutravidin (in 50 mM Tris pH
613 7.5, 200 mM NaCl, LS TBS for short) for 10 min at RT, either 10 nM (for elongation rate
614 analysis) or 3.5 nM (for side binding analysis) biotinylated inactivated heavy meromyosin (in LS
615 TBS) for 10 min at RT, washed with 20 mg/mL BSA in 50 mM Tris pH 7.5/600 mM NaCl, and
616 incubated with 20 mg/mL BSA in LS TBS for 10 min at RT. Actin was diluted to a final

617 concentration of 2.1 μM/20% Alexa-647 labeling in 1X TIRF buffer (final concentrations: 50
618 mM KCl, 2 mM $MgCl_2$, 2 mM EGTA pH 8.0, 10 mM Imidazole pH 7.0, 25 mM glucose, 1 mM
619 Trolox, 0.5% methylcellulose (400cP), 20 mM BME, 0.4 mM ATP, 20 mg/mL BSA, 0.02
620 mg/mL catalase, 0.1 mg/mL glucose oxidase, 1 mM 4-nitrobenzyl alcohol, and 0.5 mM propyl
621 gallate) and allowed to polymerize on the slide for 5 minutes at room temperature. Excess actin
622 was washed out using two 40 uL washes of TIRF buffer. A separate mixture of 1 μM actin/20%
623 Alexa-647 labeling with the indicated protein/rapamycin concentrations in 1X TIRF buffer was
624 then added to the wells and videos acquired. For unlabeled HPO-30 and CapZ experiments for
625 elongation rate analysis, the 640-nm laser was at 5% power and 50 ms exposure time with 5 s
626 intervals between frames. For the labeled CapZ experiments, the 488-nm laser was at 15% power
627 and 50 ms exposure time, the 640-nm laser was at 5% power and 50 ms exposure time, and
628 images were acquired every 500 ms in the 488-nm channel and every 20 acquisitions in the 640-
629 nm channel. For the labeled HPO-30 experiments, the 561-nm laser was at 10% power and 100
630 ms exposure time, the 640 nm laser was at 5% power and 50 ms exposure time, and images were
631 acquired every 500 ms in the 561-nm channel and every 20 acquisitions in the 640-nm channel.

632 ***smTIRF Data Processing - Actin Elongation Rate***

633 Videos were opened in ImageJ and the background removed using a rolling ball radius of
634 10 pixels. Filament length was calculated using a Gaussian-Radius of 1.5-2, determined for each
635 individual movie. The length (in microns) was converted to subunits using the established value
636 of 370 actin subunits / μm (Huxley and Brown, 1967). Time points were taken from NIS
637 Elements software. Filaments were only selected if they were present within the first 10 frames
638 of the movie and did not leave the frame during the course of the video. 10 time points were

639 selected and the length at each point was calculated, and the average slope was used for the actin
640 elongation rate.

641 ***smTIRF Data Processing - Side-binding/capping analysis***

642 Videos were opened in ImageJ and the background removed using a rolling ball radius of
643 10 pixels. Only filaments present at the beginning of the videos and those that did not leave the
644 frame during the duration of the video were selected. Side binding events were determined if
645 they met the following criteria – 1) the HPO-30/vector puncta must be present for more than one
646 frame; 2) The HPO-30/vector puncta must move with the filament at least once; 3) The filament
647 must not move away from the HPO-30/vector puncta; 4) the HPO-30/vector puncta must be
648 smaller than a circle with a radius of 4 pixels. Capping events were confirmed by the absence of
649 growth with puncta present and, if available, growth from the end capped after the puncta leaves
650 the filament.

651 ***Actin Pelleting Assays***

652 Actin pelleting assays were performed with modifications based on (Heier et al., 2017).
653 Actin was pre-polymerized at room temperature overnight by addition of 1X 50KMEH5Gd.
654 Reactions were assembled by mixing protein at 5 μM with buffer alone or buffer and actin at 2
655 μM and were allowed to bind in 50KMEH5Gd at room temperature for 30 minutes. Reactions
656 were centrifuged at 100,000 g at 4 °C for 30 min in a 42.2Ti ultracentrifuge. The supernatant was
657 removed and mixed with SDS. The pellet was dissolved by addition of G-buffer, followed by
658 brief pipetting and vortexing, and allowed to sit at room temperature for 5 min before the liquid
659 was removed and mixed with SDS. The intensity of the supernatant and pellet bands were
660 measured using ImageJ. The total intensity of the supernatant and pellet bands, and the
661 percentage of intensity from the pellet and the supernatant were calculated. The percentage

662 pelleted was calculated by subtracting the percentage of intensity from the pelleted protein in the
663 absence of actin from the percentage of intensity from the pelleted protein in the presence of
664 actin. For example, in Figure 4D, sum lanes 1 and 2 and calculate the percentage of intensity
665 from 1 and from 2. Repeat for lanes 3 and 4, then subtract the percentage intensity of lane 2 from
666 lane 4.
667

Acknowledgements

We thank ResearchIT at Iowa State University for installing AlphaFold 2 and Daniel Boesch for help with submitting prediction tasks; Aubrey Sijo-Gonzales, Finlan Rhodes, Leyuan Loh, Ganesh Prasad, Simanta Mitra, and the ResearchIT at Iowa State University for establishing web-based application (*https://biochempy.bb.iastate.edu*) for data visualization; Michael Rosen at UT Southwestern for sharing FKBP/FRB constructs; Kang Shen and Rebecca Shi at Stanford for discussions about HPO-30 function. This work was supported by funding from the National Institutes of Health (R35-GM128786) and start-up funds from the Iowa State University and the Roy J. Carver Charitable Trust to B.C., by National Institutes of Health (R35-GM136319) to B.J.N., and National Institutes of Health (R01-GM132561) to J.R.

Author contributions

B.C. conceived and oversaw the project. B.N. oversaw single molecule experiments. J.R. oversaw NMR experiments. D.A.K. purified proteins and performed biochemical experiments. D.A.K. performed AlphaFold 2 predictions. D.A.K. and J.R. performed NMR measurements. D.A.K. and H.Y.N-O. performed single molecule TIRF experiments. D.A.K. and B.C. drafted the manuscript and prepared the figures with assistance from all the authors.

Competing interests

The authors declare no competing interests.

Additional Information

Correspondence and request for materials should be addressed to stone@iastate.edu

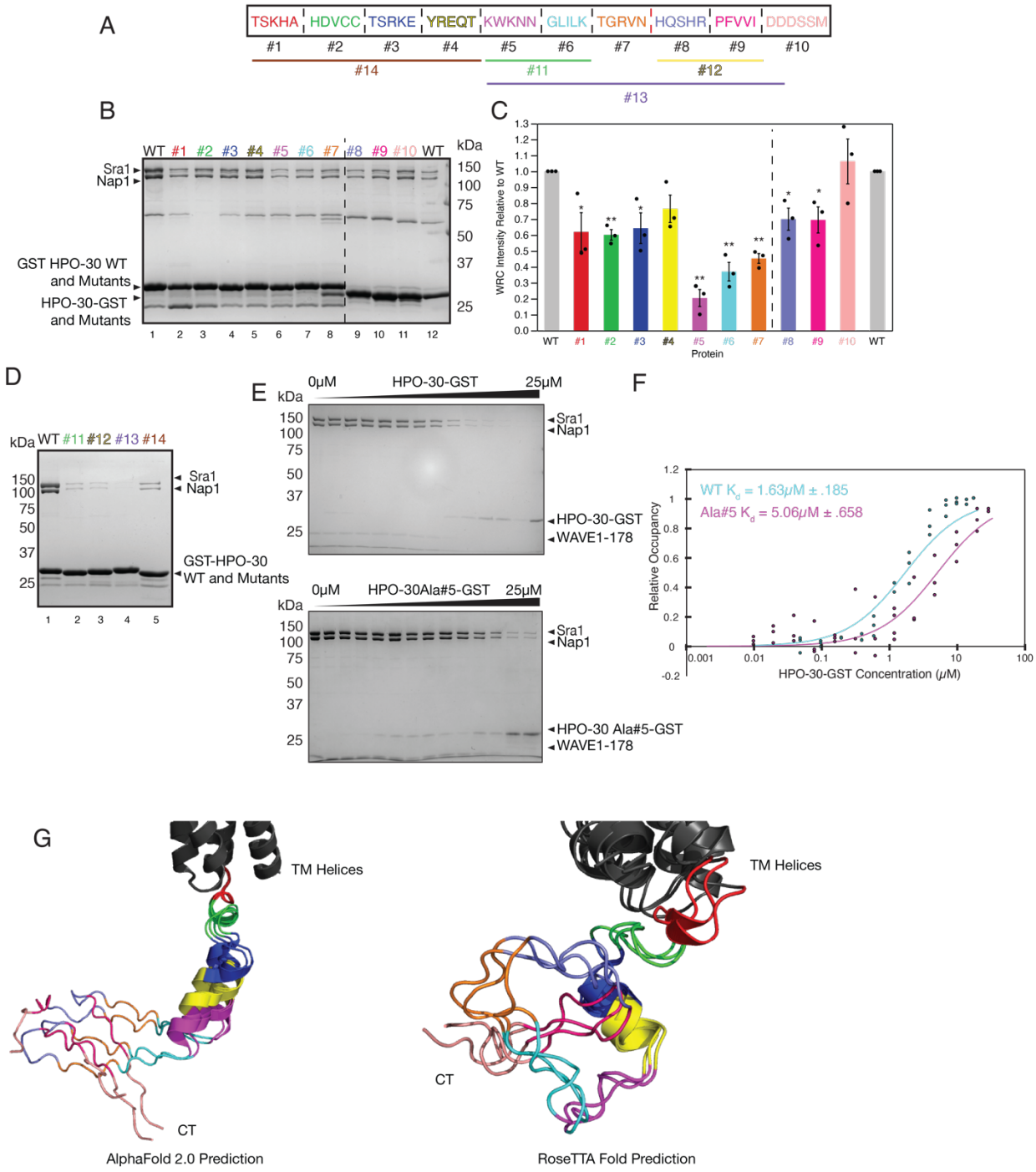

Figure 1. HPO-30 binding to WRC likely using a folded domain, rather than a linear peptide motif. A) HPO-30 ICD sequence (starting after the 4th transmembrane helix). The sequence is split into 5 AA blocks which are color coordinated to match panels B-E. Each mutation replaces the corresponding amino acids to AAAAA (for #1-10) or (GGS)n (for #11-

697 14). B) Immobilized GST-HPO-30 and HPO-30-GST constructs pulling down WRC. Mutants
698 #1-#7 and #11-14 are GST-HPO-30 constructs, mutants #8-10 are HPO-30-GST constructs. Bait
699 = 200pmol, prey = 150pmol, 50mM NaCl. Representative of three independent experiments. C)
700 Quantification of the WRC signal from the alanine scan pulldown in B. n=3 for all mutants, error
701 bars represent standard error, *=p<.05, **=p<.005 from students paired t-test. D) Immobilized
702 GST-HPO30 constructs pulling down WRC. Bait: 200pmol, Prey: 200pmol, 50mM NaCl. E)
703 Representative gel of an equilibrium pulldown of WRC using immobilized wild type (WT)
704 HPO-30-GST (top) and mutant HPO-30 Alanine #5-GST (bottom). WRC concentration was
705 0.1μM, HPO-30-GST ranged from 0 to 25μM, in 50mM NaCl. F) Data and fit curve from a one-
706 site model using Dynafit for the WT protein (cyan circles and line) and mutant Alanine #5
707 (magenta). n=3 for both WT and mutant. G) Left, structural prediction of the HPO-30 ICD in the
708 context of the full length HPO-30 protein using AlphaFold 2.0 software, with the residues color
709 coded to match A-C for the Alanine scan data. Right, structural prediction of the HPO-30 ICD in
710 the context of the full length HPO-30 protein using the RoseTTA Fold software, with the
711 residues color coded to match A-C for the Alanine scan data.
712

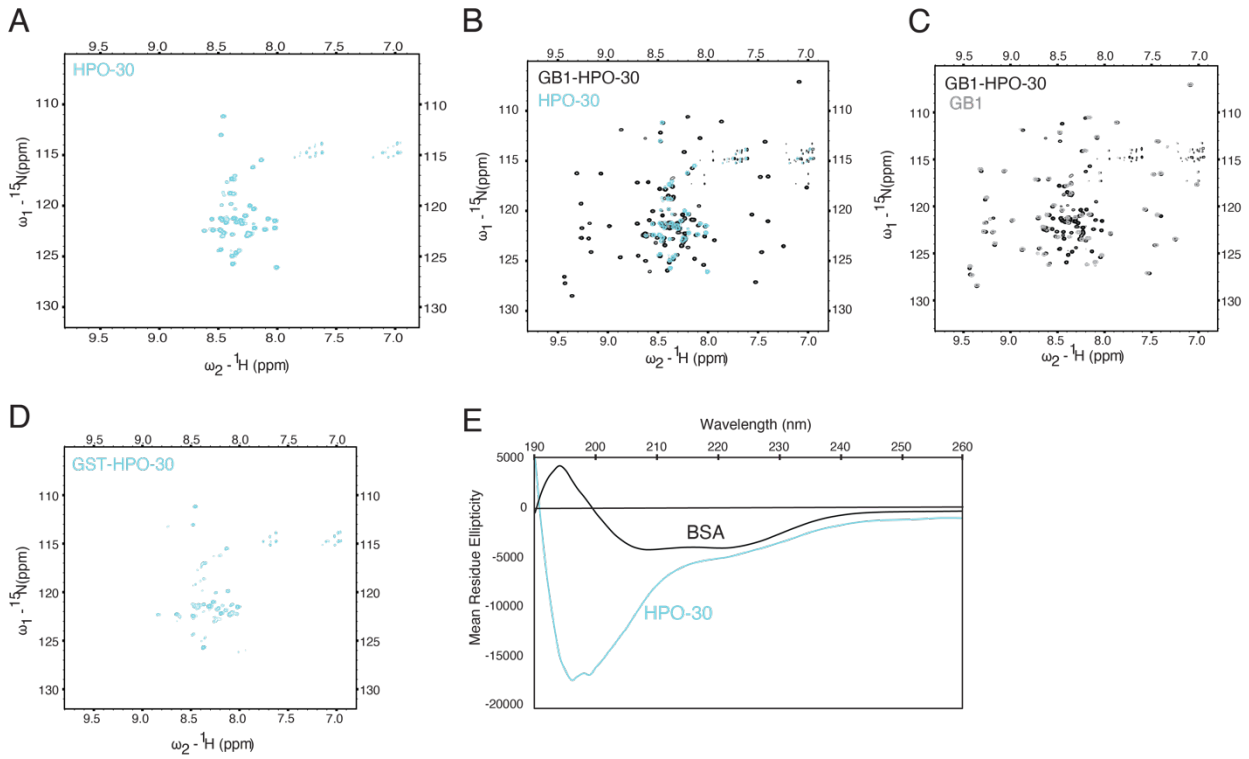

713

714 **Figure 2. HPO-30 ICD alone is unstructured.** A) 2D TROSY spectra of untagged HPO-30 in

715 100 mM NaCl, 10 mM HEPES pH 7.0, and 5% glycerol. B) 2D TROSY spectra of GB1-HPO-30

716 in 100 mM NaCl, 10 mM HEPES pH 7.0, and 5% glycerol (black) overlaid with the untagged

717 HPO-30 spectra from B (blue). C) 2D TROSY spectra of GB1-HPO-30 in 100 mM NaCl, 10

718 mM HEPES pH 7.0, and 5% glycerol (black) overlaid with the 2D TROSY spectra of GB1 tag in

719 100 mM NaCl, 10 mM HEPES pH 7.0, and 5% glycerol (gray). D) 2D HSQC spectra of GST-

720 HPO-30 in 100 mM NaCl, 10 mM HEPES pH 7.0, and 5% glycerol. E) CD spectrum of

721 untagged HPO-30 and BSA in 50KMEH5Gd.

722

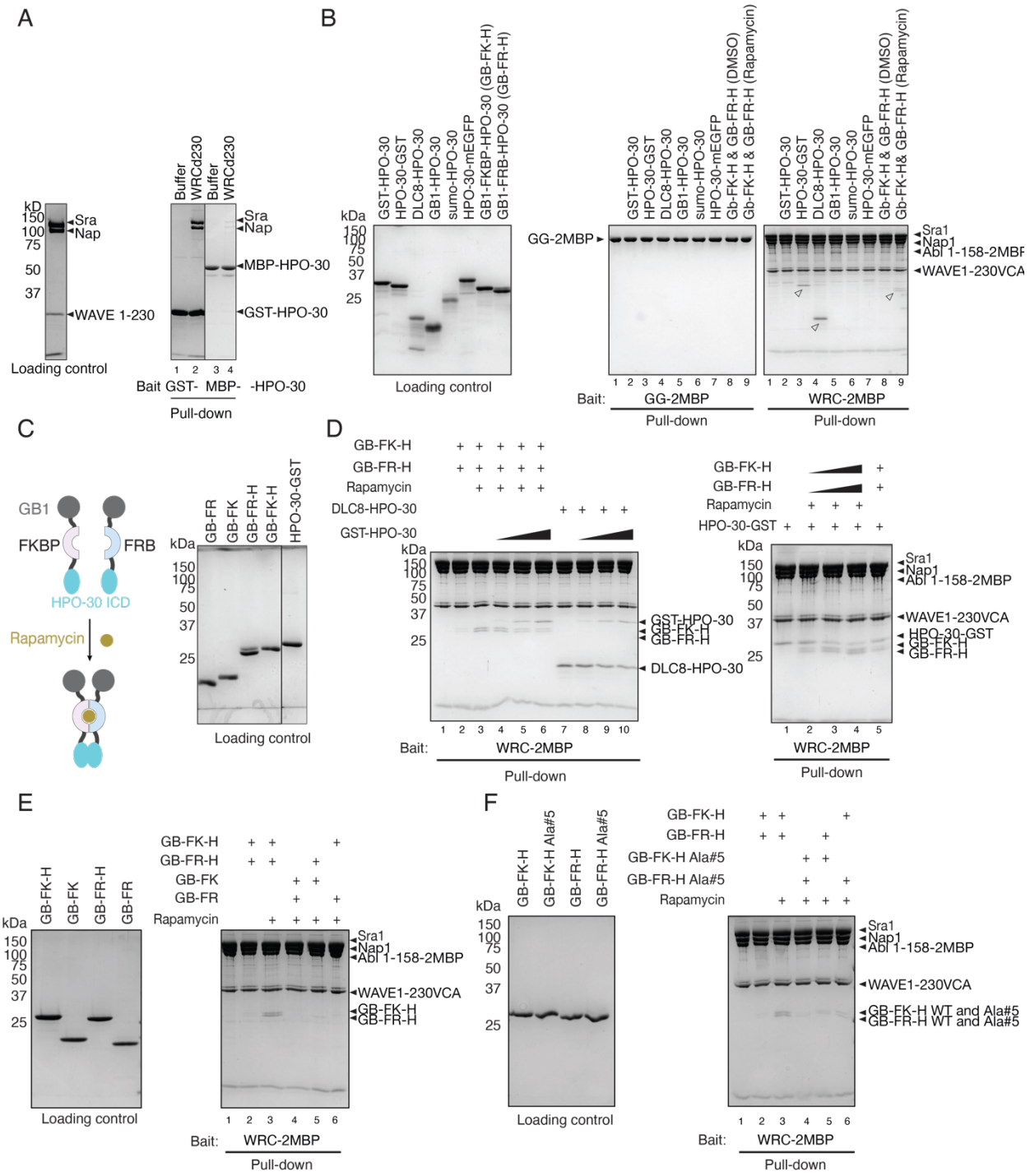

723

724 **Figure 3. HPO-30 ICD binding to the WRC is enhanced by dimerization.** A) Immobilized

725 GST-HPO-30 (GST-) and MBP-HPO-30 (MBP-) pulling down WRC. Bait: 200 pmol, Prey: 150

726 pmol, 50 mM NaCl. B) Immobilized WRC230VCA-2MBP pulling down various monomeric

727 and dimeric HPO-30. Bait: 60 pmol, Prey: 600 pmol, 50 mM NaCl, 5 uM rapamycin (or
728 equivalent volume DMSO) when noted. For clarity, GB1-FKBP-HPO30 and GB1-FRB-HPO30
729 will be shortened to GB-FK-H and GB1-FR-H, respectively. C) Cartoon schematic of
730 FKBP/FRB dimerization in the presence of rapamycin. D) Competition pulldowns using
731 immoblizied WRC230VCA-$(MBP)_2$ to pull down different combinations of dimeric HPO-30
732 constructs as bait/competitor. Bait: 60 pmol, Prey: 600 pmol, Competitor: from 600 pmol to
733 6000 pmol, 50 mM NaCl, 5 uM rapamycin (or equivalent volume DMSO) where noted. E)
734 Immobilized WRC230VCA-2MBP pulling down different combinations of GB1-FKBP/FRB
735 proteins with and without HPO-30. Bait: 60 pmol, Prey: 600 pmol for WT/WT combination,
736 1200 pmol for WT/empty, 50 mM NaCl, 5 μM rapamycin (or equivalent volume DMSO) where
737 noted. F) Immobilized WRC230VCA-2MBP pulling down different combinations of GB1-
738 FKBP/FRB proteins with and without wild type HPO-30. Bait: 60 pmol, Prey: 600 pmol for
739 WT/WT combination, 1200 pmol for WT/mutant, 50 mM NaCl, 5 μM rapamycin (or equivalent
740 volume DMSO) where noted. Note: Equal amount of FKBP/FRB proteins are added together for
741 DMSO or rapamycin samples. In the empty vector pulldowns, twice as much protein is added to
742 compensate for the loss of one functional HPO-30 moiety.
743

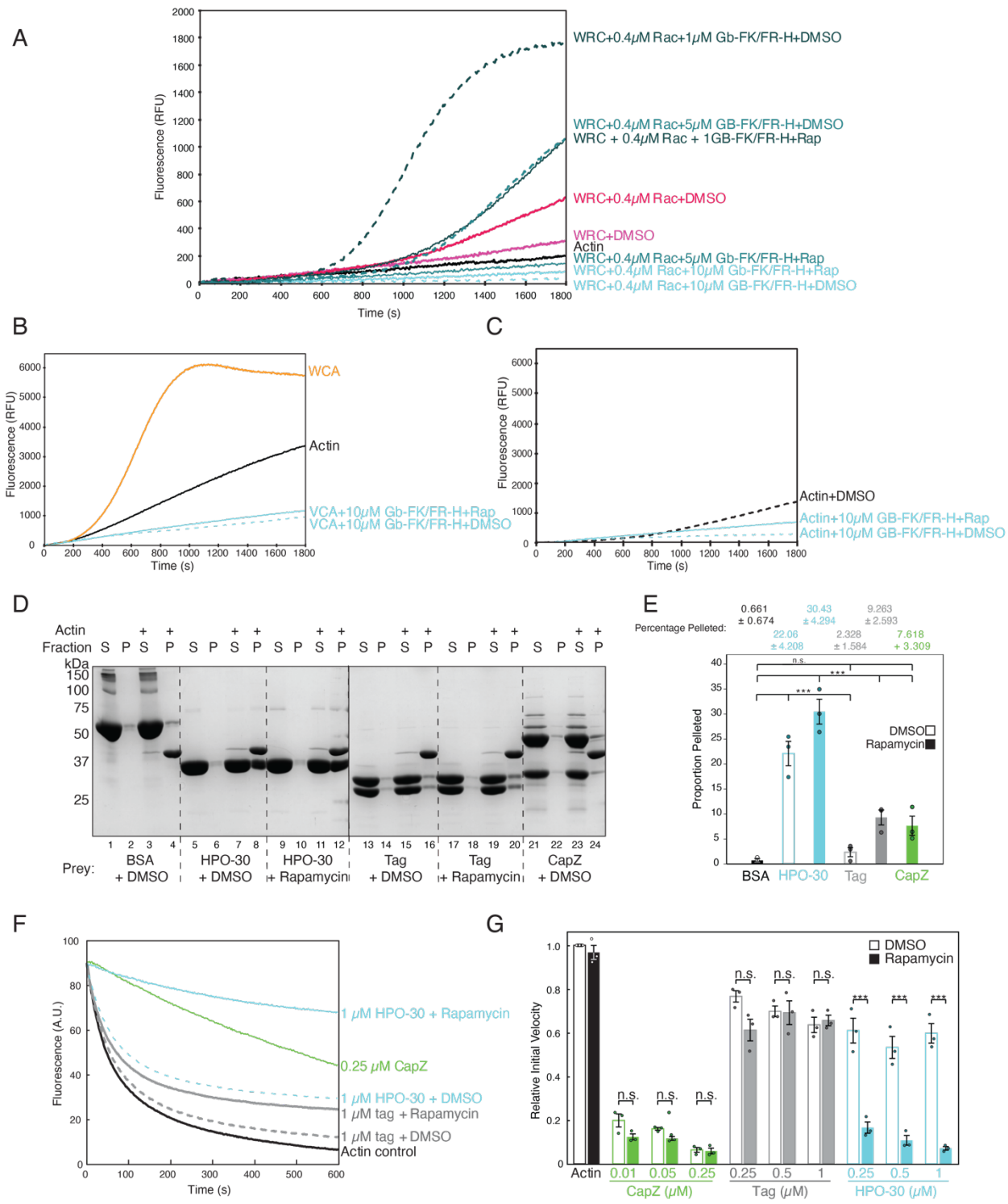

Figure 4. HPO-30 ICD binds to actin filaments and inhibits both actin polymerization and depolymerization. A) Actin polymerization assays using 4 µM actin/20% pyrene-labeling, 10

747 nM Arp2/3 complex, 100 nM WRC230VCA, and 0.4 μM Rac1 QP, and the indicated
748 concentration of equimolar GB1-FKBP-HPO-30 and GB1-FRB-HPO-30. 5 μM rapamycin or
749 equivalent volume of DMSO added. B) Actin polymerization assays using 4 μM actin/20%
750 pyrene-labeling, 10 nM Arp2/3 complex, 100 nM free WCA, and equimolar 10 μM GB1-FKBP-
751 HPO-30 and GB1-FRB-HPO-30. 5 μM rapamycin or equivalent volume of DMSO added. C)
752 Actin polymerization assays using 4 μM actin/20% pyrene-labeling, 10 nM Arp2/3 complex, and
753 equimolar 10 μM GB1-FKBP-HPO-30 and GB1-FRB-HPO-30. 5 μM rapamycin or equivalent
754 volume of DMSO added. D) Actin pelleting assays with monomeric and dimeric HPO-30 and
755 CapZ. S= supernatant, P= pellet. Representative gel from three replicates. E) Quantification of
756 the percentage of protein found in the pellet from D. Bars represent standard error, n = 3, ** =
757 p<.01, *** = p<.001 from ANOVA on ranks and Tukey test. F) Representative depolymerization
758 assay fluorescence curves for one concentration of CapZ, SNAP-FKBP-HPO-30/SNAP-FRB-
759 HPO-30 (labeled as "HPO-30"), and SNAP-FKBP/SNAP-FRB (labeled as "Tag"). G)
760 Quantification of relative initial velocity from fluorescence curves in D, error bars represent
761 standard error, n=3, *** = p<.001 from ANOVA on ranks and Tukey test. 5 μM actin diluted 20-
762 fold into 25% 50KMEH5Gd/75%GMg with or without the indication protein. 5 μM rapamycin
763 or equivalent volume of DMSO was added.
764

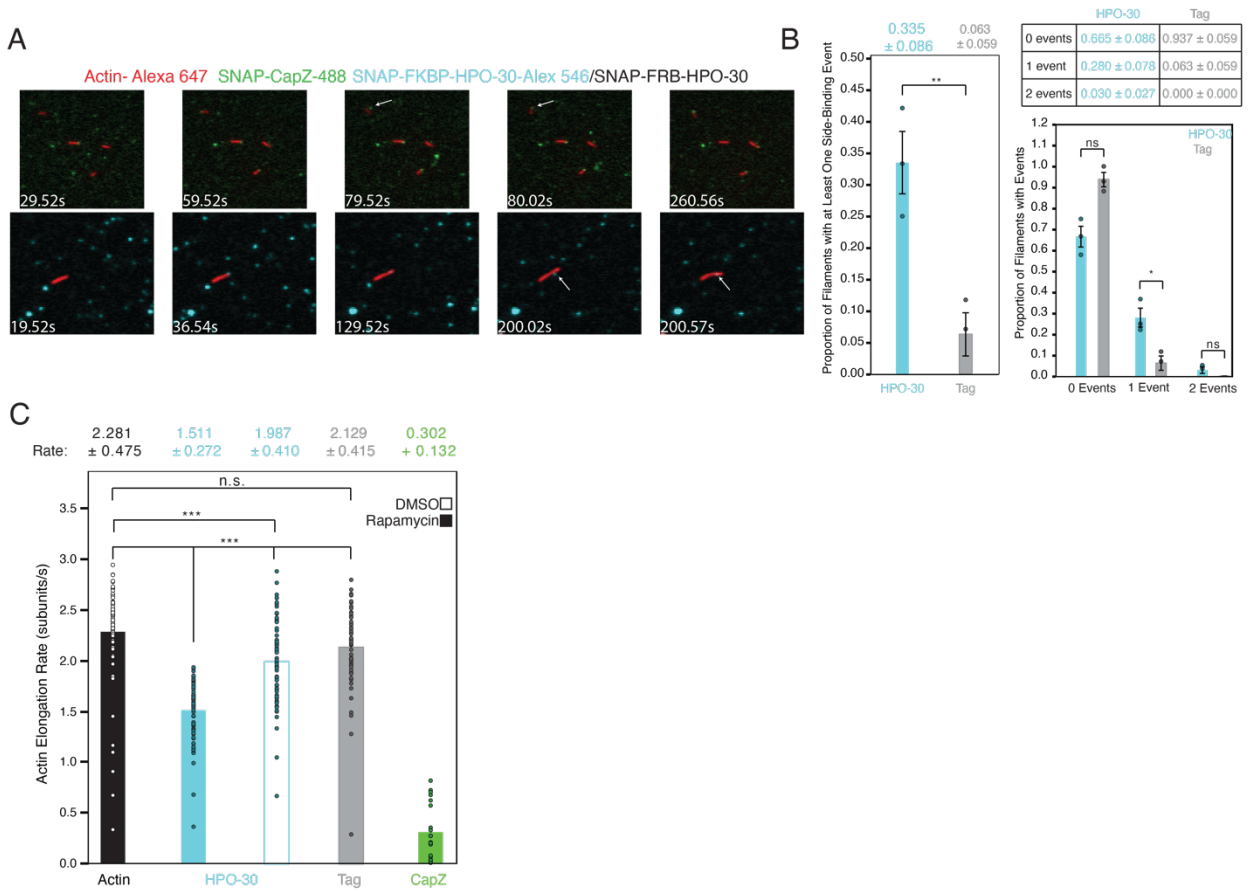

Figure 5. HPO-30 ICD binds to the side of actin filaments and slows down actin polymerization. A) Top, still frames of several capping events between SNAP-CapZ-488 (5nM, green) and actin (red). Bottom, still frames of a side-binding event between SNAP-FKBP-HPO-30-546/SNAP-FRB-HPO-30 (15nM, cyan) and actin (red). The images in top and bottom are not to the same scale. B) Left, Quantification of the frequency of side binding events from smTIRF videos. Right, quantification of the frequency of filaments with 0 events, 1 event, and 2 events. n=3 videos, at least 15 filaments per video. * = p< .05, ** = p< .01 from students paired t-test. Bars represent standard error. C) Quantification of elongation rate of actin filaments in smTIRF videos. n = 78 filaments from two independent videos for actin, n = 82 filaments from four independent videos for HPO-30 + rapamycin, n = 71 filaments from four independent videos for

776 HPO-30 + DMSO, n = 54 filaments from three independent videos for tag + rapamycin, n = 19

777 filaments from one video for CapZ. *** = p<.001 from ANOVA on ranks and Tukey test.

778

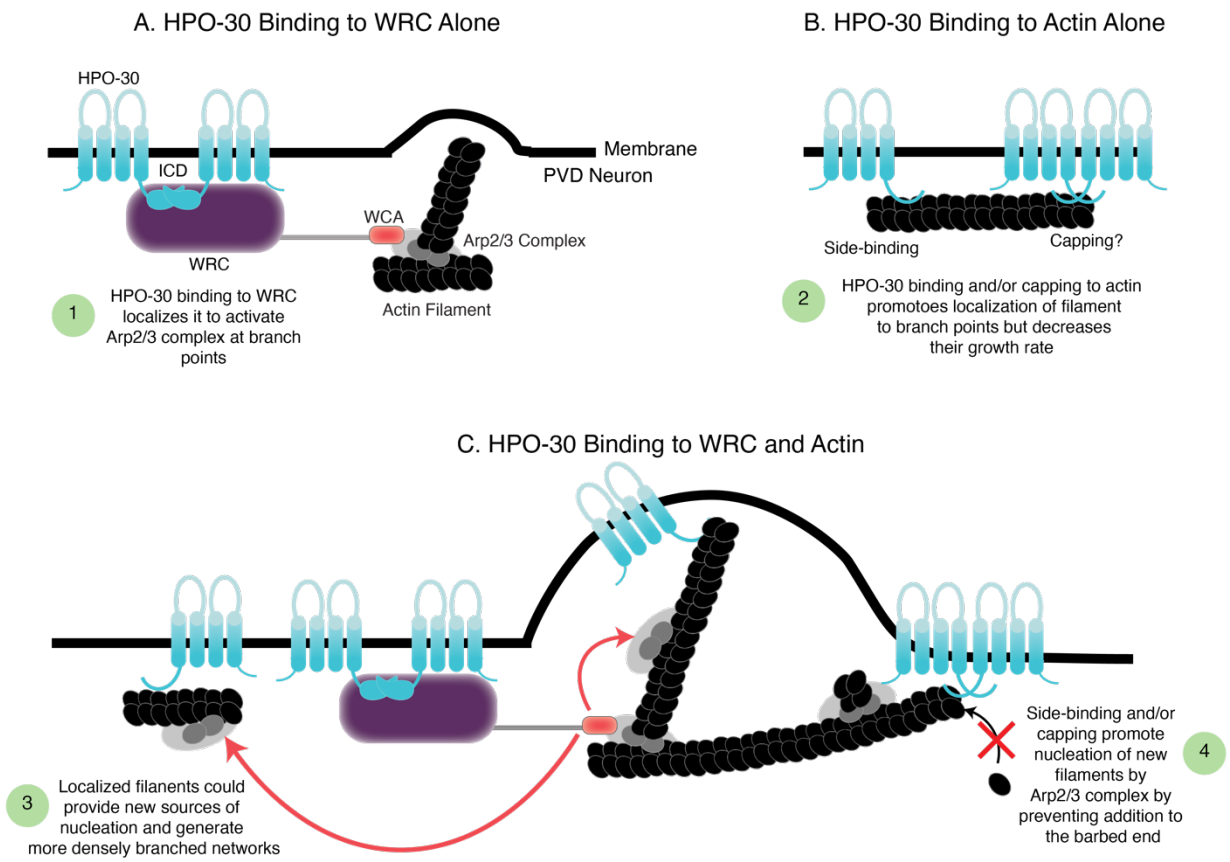

Figure 6. Model showing how the dual functions of HPO-30 ICD in binding WRC and actin can fine tune local actin dynamics. A) HPO-30 binding to the WRC alone promotes local actin polymerization via the WRC-Arp2/3 complex pathway. B) HPO-30 binding to actin filaments alone promotes localization of the filaments, but causes a decrease in their polymerization speed. C) HPO-30 binding to both the WRC and to actin would promote local actin polymerization via the WRC-Arp2/3 pathway, and would stimulate the formation of a more densely branched filament network by preventing elongation of filaments and the nucleation of daughter filaments by the Arp2/3 complex. Localization of the WRC would further stimulate new branch points by the Arp2/3 complex.

Supplemental materials

Supplemental Table 1: Sequences of recombinant proteins used in this study.

Construct name	Description	Sequence	Source or reference
GST-HPO30	GST-thrombin-TEV-ceHPO-30 ICD (a.a. 229-279)	MSPILGYWKIKGLVQPTRLLLEYLEEKYEEHLYERDEGDKWRNKKFELGLEFPN LPYYIDGDVKLTQSMAIIRYIADKHNMLGGCPKERAEISMLEGAVLDIRYGVSRI AYSKDFETLKVDFLSKLPEMLKMFEDRLCHKTYLNGDHVTHPDFMLYDALDV VLYMDPMCLDAFPKLVCFKKRIEAIPQIDKYLKSSKYIAWPLQGWQATFGGGD HPPKSDLVPRGSENLYFQGHMTSKHAHDVCCTSRKEYREQTKWKNNGLILKTG RVNHQSHRPFVVIDDDSSM	Zou, 2018
GST-HPO30 Ala #1	GST-thrombin-TEV-ceHPO-30 ICD Ala 229-233	MSPILGYWKIKGLVQPTRLLLEYLEEKYEEHLYERDEGDKWRNKKFELGLEFPN LPYYIDGDVKLTQSMAIIRYIADKHNMLGGCPKERAEISMLEGAVLDIRYGVSRI AYSKDFETLKVDFLSKLPEMLKMFEDRLCHKTYLNGDHVTHPDFMLYDALDV VLYMDPMCLDAFPKLVCFKKRIEAIPQIDKYLKSSKYIAWPLQGWQATFGGGD HPPKSDLVPRGSENLYFQGHMAAAAAHDVCCTSRKEYREQTKWKNNGLILKTG RVNHQSHRPFVVIDDDSSM	Zou, 2018
GST-HPO30 Ala #2	GST-thrombin-TEV-ceHPO-30 ICD Ala 234-238	MSPILGYWKIKGLVQPTRLLLEYLEEKYEEHLYERDEGDKWRNKKFELGLEFPN LPYYIDGDVKLTQSMAIIRYIADKHNMLGGCPKERAEISMLEGAVLDIRYGVSRI AYSKDFETLKVDFLSKLPEMLKMFEDRLCHKTYLNGDHVTHPDFMLYDALDV VLYMDPMCLDAFPKLVCFKKRIEAIPQIDKYLKSSKYIAWPLQGWQATFGGGD HPPKSDLVPRGSENLYFQGHMTSKHAAAAAATSRKEYREQTKWKNNGLILKTG RVNHQSHRPFVVIDDDSSM	Zou, 2018
GST-HPO30 Ala #3	GST-thrombin-TEV-ceHPO-30 ICD Ala 239-243	MSPILGYWKIKGLVQPTRLLLEYLEEKYEEHLYERDEGDKWRNKKFELGLEFPN LPYYIDGDVKLTQSMAIIRYIADKHNMLGGCPKERAEISMLEGAVLDIRYGVSRI AYSKDFETLKVDFLSKLPEMLKMFEDRLCHKTYLNGDHVTHPDFMLYDALDV VLYMDPMCLDAFPKLVCFKKRIEAIPQIDKYLKSSKYIAWPLQGWQATFGGGD HPPKSDLVPRGSENLYFQGHMTSKHAHDVCCAAAAAYREQTKWKNNGLILKT GRVNHQSHRPFVVIDDDSSM	Zou, 2018
GST-HPO30 Ala #4	GST-thrombin-TEV-ceHPO-30 ICD Ala 244-248	MSPILGYWKIKGLVQPTRLLLEYLEEKYEEHLYERDEGDKWRNKKFELGLEFPN LPYYIDGDVKLTQSMAIIRYIADKHNMLGGCPKERAEISMLEGAVLDIRYGVSRI AYSKDFETLKVDFLSKLPEMLKMFEDRLCHKTYLNGDHVTHPDFMLYDALDV VLYMDPMCLDAFPKLVCFKKRIEAIPQIDKYLKSSKYIAWPLQGWQATFGGGD HPPKSDLVPRGSENLYFQGHMTSKHAHDVCCTSRKEAAAAAKWKNNGLILKTG RVNHQSHRPFVVIDDDSSM	Zou, 2018
GST-HPO30 Ala #5	GST-thrombin-TEV-ceHPO-30 ICD Ala 249-253	MSPILGYWKIKGLVQPTRLLLEYLEEKYEEHLYERDEGDKWRNKKFELGLEFPN LPYYIDGDVKLTQSMAIIRYIADKHNMLGGCPKERAEISMLEGAVLDIRYGVSRI AYSKDFETLKVDFLSKLPEMLKMFEDRLCHKTYLNGDHVTHPDFMLYDALDV VLYMDPMCLDAFPKLVCFKKRIEAIPQIDKYLKSSKYIAWPLQGWQATFGGGD HPPKSDLVPRGSENLYFQGHMTSKHAHDVCCTSRKEYREQTAAAAAGLILKTG RVNHQSHRPFVVIDDDSSM	Zou, 2018
GST-HPO30 Ala #6	GST-thrombin-TEV-ceHPO-30 ICD Ala 254-258	MSPILGYWKIKGLVQPTRLLLEYLEEKYEEHLYERDEGDKWRNKKFELGLEFPN LPYYIDGDVKLTQSMAIIRYIADKHNMLGGCPKERAEISMLEGAVLDIRYGVSRI AYSKDFETLKVDFLSKLPEMLKMFEDRLCHKTYLNGDHVTHPDFMLYDALDV VLYMDPMCLDAFPKLVCFKKRIEAIPQIDKYLKSSKYIAWPLQGWQATFGGGD HPPKSDLVPRGSENLYFQGHMTSKHAHDVCCTSRKEYREQTKWKNNAAAAAT GRVNHQSHRPFVVIDDDSSM	Zou, 2018
GST-HPO30 Ala #7	GST-thrombin-TEV-ceHPO-30 ICD Ala 259-263	MSPILGYWKIKGLVQPTRLLLEYLEEKYEEHLYERDEGDKWRNKKFELGLEFPN LPYYIDGDVKLTQSMAIIRYIADKHNMLGGCPKERAEISMLEGAVLDIRYGVSRI AYSKDFETLKVDFLSKLPEMLKMFEDRLCHKTYLNGDHVTHPDFMLYDALDV VLYMDPMCLDAFPKLVCFKKRIEAIPQIDKYLKSSKYIAWPLQGWQATFGGGD HPPKSDLVPRGSENLYFQGHMTSKHAHDVCCTSRKEYREQTKWKNNGLILKAA AAAHQSHRPFVVIDDDSSM	Zou, 2018
HPO30-GST	ceHPO-30 ICD (a.a. 229-279)-GG-3C-GST	MTSKHAHDVCCTSRKEYREQTKWKNNGLILKTGRVNHQSHRPFVVIDDDSSMG GLEVLFQGPMSPILGYWKIKGLVQPTRLLLEYLEEKYEEHLYERDEGDKWRNK KFELGLEFPNLPYYIDGDVKLTQSMAIIRYIADKHNMLGGCPKERAEISMLEGAV LDIRYGVSRIAYSKDFETLKVDFLSKLPEMLKMFEDRLCHKTYLNGDHVTHPDF MLYDALDVVLYMDPMCLDAFPKLVCFKKRIEAIPQIDKYLKSSKYIAWPLQGW QATFGGGDHPPK	This paper
HPO30 Ala #8 - GST	ceHPO-30 ICD Ala 264-268	MTSKHAHDVCCTSRKEYREQTKWKNNGLILKTGRVNAAAAAPFVVIDDDSSM GGLEVLFQGPMSPILGYWKIKGLVQPTRLLLEYLEEKYEEHLYERDEGDKWRN KKFELGLEFPNLPYYIDGDVKLTQSMAIIRYIADKHNMLGGCPKERAEISMLEGA VLDIRYGVSRIAYSKDFETLKVDFLSKLPEMLKMFEDRLCHKTYLNGDHVTHPD FMLYDALDVVLYMDPMCLDAFPKLVCFKKRIEAIPQIDKYLKSSKYIAWPLQG WQATFGGGDHPPK	This paper

HPO30 Ala #9 - GST	ceHPO-30 ICD Ala 269-273	MTSKHAHDVCCTSRKEYREQTKWKNNGLILKTGRVNHQSHRAAAAADDDSSM GGLEVLFQGPMSPILGYWKIKGLVQPTRLLLEYLEEKYEEHLYERDEGDKWRN KKFELGLEFPNLPYYIDGDVKLTQSMAIIRYIADKHNMLGGCPKERAEISMLEGA VLDIRYGVSRIAYSKDFETLKVDFLSKLPEMLKMFEDRLCHKTYLNGDHVTHPD FMLYDALDVVLYMDPMCLDAFPKLVCFKKRIEAIPQIDKYLKSSKYIAWPLQG WQATFGGGDHPPK	This paper
HPO30 Ala #10 - GST	ceHPO-30 ICD Ala 274-279	MTSKHAHDVCCTSRKEYREQTKWKNNGLILKTGRVNHQSHRPFVVIAAAAAA GGLEVLFQGPMSPILGYWKIKGLVQPTRLLLEYLEEKYEEHLYERDEGDKWRN KKFELGLEFPNLPYYIDGDVKLTQSMAIIRYIADKHNMLGGCPKERAEISMLEGA VLDIRYGVSRIAYSKDFETLKVDFLSKLPEMLKMFEDRLCHKTYLNGDHVTHPD FMLYDALDVVLYMDPMCLDAFPKLVCFKKRIEAIPQIDKYLKSSKYIAWPLQG WQATFGGGDHPPK	This paper
GST-HPO30 GGS #11	GST-thrombin-TEV-ceHPO-30 ICD GGS 249-258	MSPILGYWKIKGLVQPTRLLLEYLEEKYEEHLYERDEGDKWRNKKFELGLEFPN LPYYIDGDVKLTQSMAIIRYIADKHNMLGGCPKERAEISMLEGAVLDIRYGVSRI AYSKDFETLKVDFLSKLPEMLKMFEDRLCHKTYLNGDHVTHPDFMLYDALDV VLYMDPMCLDAFPKLVCFKKRIEAIPQIDKYLKSSKYIAWPLQGWQATFGGGD HPPKSDLVPRGSENLYFQGHMTSKHAHDVCCTSRKEYREQTGGSGGSGGSGTG RVNHQSHRPFVVIDDDSSM	This paper
GST-HPO30 GGS #12	GST-thrombin-TEV-ceHPO-30 ICD GGS 264-273	MSPILGYWKIKGLVQPTRLLLEYLEEKYEEHLYERDEGDKWRNKKFELGLEFPN LPYYIDGDVKLTQSMAIIRYIADKHNMLGGCPKERAEISMLEGAVLDIRYGVSRI AYSKDFETLKVDFLSKLPEMLKMFEDRLCHKTYLNGDHVTHPDFMLYDALDV VLYMDPMCLDAFPKLVCFKKRIEAIPQIDKYLKSSKYIAWPLQGWQATFGGGD HPPKSDLVPRGSENLYFQGHMTSKHAHDVCCTSRKEYREQTKWKNNAAAAAT GRVNGGSGGSGGSGDDDSSM	This paper
GST-HPO30 GGS #13	GST-thrombin-TEV-ceHPO-30 ICD GGS 264-275	MSPILGYWKIKGLVQPTRLLLEYLEEKYEEHLYERDEGDKWRNKKFELGLEFPN LPYYIDGDVKLTQSMAIIRYIADKHNMLGGCPKERAEISMLEGAVLDIRYGVSRI AYSKDFETLKVDFLSKLPEMLKMFEDRLCHKTYLNGDHVTHPDFMLYDALDV VLYMDPMCLDAFPKLVCFKKRIEAIPQIDKYLKSSKYIAWPLQGWQATFGGGD HPPKSDLVPRGSENLYFQGHMTSKHAHDVCCTSRKEYREQTGGSGGSGGSGGS GGSGGSGGSGGSGGSDSSM	This paper
GST-HPO30 GGS #14	GST-thrombin-TEV-ceHPO-30 ICD GGS 229-248	MSPILGYWKIKGLVQPTRLLLEYLEEKYEEHLYERDEGDKWRNKKFELGLEFPN LPYYIDGDVKLTQSMAIIRYIADKHNMLGGCPKERAEISMLEGAVLDIRYGVSRI AYSKDFETLKVDFLSKLPEMLKMFEDRLCHKTYLNGDHVTHPDFMLYDALDV VLYMDPMCLDAFPKLVCFKKRIEAIPQIDKYLKSSKYIAWPLQGWQATFGGGD HPPKSDLVPRGSENLYFQGHMGGSGGSGGSGGSGGSGGSGGKWKNNGLILKTG RVNHQSHRPFVVIDDDSSM	This paper
HPO30-mEGFP	GST-TEV-ceHPO-30 ICD 229-279 – GGS2-mEGFP, GST tag removed by TEV cleavage	MSPILGYWKIKGLVQPTRLLLEYLEEKYEEHLYERDEGDKWRNKKFELGLEFPN LPYYIDGDVKLTQSMAIIRYIADKHNMLGGCPKERAEISMLEGAVLDIRYGVSRI AYSKDFETLKVDFLSKLPEMLKMFEDRLCHKTYLNGDHVTHPDFMLYDALDV VLYMDPMCLDAFPKLVCFKKRIEAIPQIDKYLKSSKYIAWPLQGWQATFGGGD HPPKSDLVPRGSENLYFQGHMTSKHAHDVCCTSRKEYREQTKWKNNGLILKTG RVNHQSHRPFVVIDDDSSMGGSGGSMVSKGEELFTGVVPILVELDGDVNGHKFS VSGEGEGDATYGKLTLKFICTTGKLPVPWPTLVTTLTYGVQCFSRYPDHMKQH DFFKSAMPEGYVQERTIFFKDDGNYKTRAEVKFEGDTLVNRIELKGIDFKEDGNI LGHKLEYNYNSHNVYIMADKQKNGIKVNFKIRHNIEDGSVQLADHYQQNTPIG DGPVLLPDNHYLSTQSKLSKDPNEKRDHMVLKEKVTAAGITLGMDELYK	This paper
HPO30	MBP-TEV-ceHPO-30 ICD 229-279, MBP tag removed by TEV cleavage	MKIEEGKLVIWINGDKGYNGLAEVGKKFEKDTGIKVTVEHPDKLEEKFPQVAAT GDGPDIIFWAHDRFGGYAQSGLLAEITPDKAFQDKLYPFTWDAVRYNGKLIAYP IAVEALSLIYNKDLLPNPPKTWEEIPALDKELKAKGKSALMFNLQEPYFTWPLIA ADGGYAFKYENGKYDIKDVGVDNAGAKAGLTFLVDLIKNKHMNADTDYSIAE AAFNKGETAMTINGPWAWSNIDTSKVNYGVTVLPTFKGQPSKPFVGVLSAGINA ASPNKELAKEFLENYLLTDEGLEAVNKDKPLGAVALKSYEEELAKDPRIAATME NAQKGEIMPNIPQMSAFWYAVRTAVINAASGRQTVDEALKDAQTNSSSNNNNN NNNNNLGIEGRISEFENLYFQGHTSKHAHDVCCTSRKEYREQTKWKNNGLILKT GRVNHQSHRPFVVIDDDSSM	This paper
DLC8-HPO30	DLC8-TEV-ceHPO-30 ICD 229-279-His6	MSDRKAVIKNADMSEEMQQDAVDCATQALEKYNIEKDIAAYIKKEFDKKYNPT WHCIVGRNFGSYVTHETRHFIYFYLGQVAILLFKSGGSENLYFQGHMTSKHAHD VCCTSRKEYREQTKWKNNGLILKTGRVNHQSHRPFVVIDDDSSMHHHHHH	This paper
GB1-HPO30	GB1-thrombin-ceHPO-30 ICD 229-279-His6	MQYKLALNGKTLKGETTTEAVDAATAEKVFKQYANDNGVDGEWTYDDATKT FTVTELVPRGSTSKHAHDVCCTSRKEYREQTKWKNNGLILKTGRVNHQSHRPF VVIDDDSSMHHHHHH	This paper
sumo-HPO30	His10-Sumo-GGS-ceHPO-30 ICD 229-279	MGHHHHHHHHHHSSGHIEGRHMASMSDSEVNQEAKPEVKPEVKPETHINLKVS DGSSEIFFKIKKTTPLRRLMEAFAKRQGKEMDSLRFLYDGIRIQADQTPEDLDME DNDIIEAHREQIGGSTSKHAHDVCCTSRKEYREQTKWKNNGLILKTGRVNHQSH RPFVVIDDDSSM	This paper

GB1-FKBP-HPO30	GB1-thrombin-FKBP-GGS3-ceHPO-30 ICD 229-279 – His6	MQYKLALNGKTLKGETTTEAVDAATAEKVFKQYANDNGVDGEWTYDDATKTFTVTELVPRGSHMVQVETISPGDGRTFPKRGQTCVVHYTGMLEDGKKFDSSRDRNKPFKFMLGKQEVIRGWEEGVAQMSVGQRAKLTISPDYAYGATGHPGIIPPHATLVFDVELLKLEGGSGGSGGSMTSKHAHDVCCTSRKEYREQTKWKNNGLILKTGRVNHQSHRPFVVIDDDSSMHHHHHH	This paper
GB1-FRB-HPO30	GB1-thrombin-FRB-GGS3-ceHPO-30 ICD 229-279 – His6	MQYKLALNGKTLKGETTTEAVDAATAEKVFKQYANDNGVDGEWTYDDATKTFTVTELVPRGSHMELIRVAILWHEMWHEGLEEASRLYFGERNVKGMFEVLEPLHAMMERGPQTLKETSFNQAYGRDLMEAQEWCRKYMKSGNVKDLTQAWDLYYHVFRRISKQGGSGGSGGSM**T**SKHAHDVCCTSRKEYREQTKWKNNGLILKTGRVNHQSHRPFVVIDDDSS**M**HHHHHH	This paper
GB1-FKBP	GB1-thrombin-FKBP-GGS3-His6	MQYKLALNGKTLKGETTTEAVDAATAEKVFKQYANDNGVDGEWTYDDATKTFTVTELVPRGSHMVQVETISPGDGRTFPKRGQTCVVHYTGMLEDGKKFDSSRDRNKPFKFMLGKQEVIRGWEEGVAQMSVGQRAKLTISPDYAYGATGHPGIIPPHATLVFDVELLKLEGGSGGSGGSHHHHHH	This paper
GB1-FRB	GB1-thrombin-FRB-GGS3-His6	MQYKLALNGKTLKGETTTEAVDAATAEKVFKQYANDNGVDGEWTYDDATKTFTVTELVPRGSHMELIRVAILWHEMWHEGLEEASRLYFGERNVKGMFEVLEPLHAMMERGPQTLKETSFNQAYGRDLMEAQEWCRKYMKSGNVKDLTQAWDLYYHVFRRISKQGGSGGSGGSHHHHHH	This paper
GB1-FKBP-HPO30 Ala #5	GB1-thrombin-FKBP-GGS3-ceHPO-30 ICD Ala 249-253– His6	MQYKLALNGKTLKGETTTEAVDAATAEKVFKQYANDNGVDGEWTYDDATKTFTVTELVPRGSHMVQVETISPGDGRTFPKRGQTCVVHYTGMLEDGKKFDSSRDRNKPFKFMLGKQEVIRGWEEGVAQMSVGQRAKLTISPDYAYGATGHPGIIPPHATLVFDVELLKLEGGSGGSGGSMTSKHAHDVCCTSRKEYREQTAAAAAGLILKTGRVNHQSHRPFVVIDDDSSMHHHHHH	This paper
GB1-FRB-HPO30 Ala #5	GB1-FRB-thrombin-GGS3-ceHPO-30 ICD Ala 249-253– His6	QYKLALNGKTLKGETTTEAVDAATAEKVFKQYANDNGVDGEWTYDDATKTFTVTELVPRGSHMELIRVAILWHEMWHEGLEEASRLYFGERNVKGMFEVLEPLHAMMERGPQTLKETSFNQAYGRDLMEAQEWCRKYMKSGNVKDLTQAWDLYYHVFRRISKQGGSGGSGGSMTSKHAHDVCCTSRKEYREQTAAAAAGLILKTGRVNHQSHRPFVVIDDDSSMHHHHHH	This paper
SNAP-FKBP-HPO30	SNAP-FKBP-GGS3-ceHPO-30 ICD 229-279-His6	MDKDCEMKRTTLDSPLGKLELSGCEQGLHEIKLLGKGTSAADAVEVPAPAAVLGGPEPLMQATAWLNAYFHQPEAIEEFPVPALHHPVFQQESFTRQVLWKLLKVVKFGEVISYQQLAALAGNPAATAAVKTALSGNPVPILIPCHRVVSSSGAAGGYEGGLAVKEWLLAHEGHRLGKPGLGPAGIGAPGSMVQVETISPGDGRTFPKRGQTCVVHYTGMLEDGKKFDSSRDRNKPFKFMLGKQEVIRGWEEGVAQMSVGQRAKLTISPDYAYGATGHPGIIPPHATLVFDVELLKLEGGSGGSGGSMTSKHAHDVCCTSRKEYREQTKWKNNGLILKTGRVNHQSHRPFVVIDDDSSMHHHHHH	https://www.addgene.org/101137/ and this paper
SNAP-FRB-HPO30	SNAP-FRB-GGS3-ceHPO-30 ICD 229-279-His6	MDKDCEMKRTTLDSPLGKLELSGCEQGLHEIKLLGKGTSAADAVEVPAPAAVLGGPEPLMQATAWLNAYFHQPEAIEEFPVPALHHPVFQQESFTRQVLWKLLKVVKFGEVISYQQLAALAGNPAATAAVKTALSGNPVPILIPCHRVVSSSGAVGGYEGGLAVKEWLLAHEGHRLGKPGLGPAGIGAPGSMELIRVAILWHEMWHEGLEEASRLYFGERNVKGMFEVLEPLHAMMERGPQTLKETSFNQAYGRDLMEAQEWCRKYMKSGNVKDLTQAWDLYYHVFRRISKQGGSGGSGGSMTSKHAHDVCCTSRKEYREQTKWKNNGLILKTGRVNHQSHRPFVVIDDDSSMHHHHHH	https://www.addgene.org/101137/ and this paper
SNAP-FKBP	SNAP-FKBP-GGS3-His6	MDKDCEMKRTTLDSPLGKLELSGCEQGLHEIKLLGKGTSAADAVEVPAPAAVLGGPEPLMQATAWLNAYFHQPEAIEEFPVPALHHPVFQQESFTRQVLWKLLKVVKFGEVISYQQLAALAGNPAATAAVKTALSGNPVPILIPCHRVVSSSGAVGGYEGGLAVKEWLLAHEGHRLGKPGLGPAGIGAPGSMVQVETISPGDGRTFPKRGQTCVVHYTGMLEDGKKFDSSRDRNKPFKFMLGKQEVIRGWEEGVAQMSVGQRAKLTISPDYAYGATGHPGIIPPHATLVFDVELLKLEGGSGGSGGSHHHHHH	https://www.addgene.org/101137/ and this paper
SNAP-FRB	SNAP-FRB-GGS3-His6	MDKDCEMKRTTLDSPLGKLELSGCEQGLHEIKLLGKGTSAADAVEVPAPAAVLGGPEPLMQATAWLNAYFHQPEAIEEFPVPALHHPVFQQESFTRQVLWKLLKVVKFGEVISYQQLAALAGNPAATAAVKTALSGNPVPILIPCHRVVSSSGAVGGYEGGLAVKEWLLAHEGHRLGKPGLGPAGIGAPGSMELIRVAILWHEMWHEGLEEASRLYFGERNVKGMFEVLEPLHAMMERGPQTLKETSFNQAYGRDLMEAQEWCRKYMKSGNVKDLTQAWDLYYHVFRRISKQGGSGGSGGSHHHHHH	https://www.addgene.org/101137/ and this paper
SNAP-CapZ	His9-SNAP-CapZ β / CapZ α, from *Gallus gallus*	MGHHHHHHHHHHENLYFQGSEFMDKDCEMKRTTLDSPLGKLELSGCEQGLHEIKLLGKGTSAADAVEVPAPAAVLGGPEPLMQATAWLNAYFHQPEAIEEFPVPALHHPVFQQESFTRQVLWKLLKVVKFGEVISYQQLAALAGNPAATAAVKTALSGNPVPILIPCHRVVSSSGAVGGYEGGLAVKEWLLAHEGHRLGKPGLGPAGIGAPGSMSDQQLDCALDLMRRLPPQQIEKNLSDLIDLVPSLCEDLLSSVDQPLKIARDKVVGKDYLLCDYNRDGDSYRSPWSNKYDPPLEDGAMPSARLRKLEVEANNAFDQYRDLYFEGGVSSVYLWDLDHGFAGVILIKKAGDGSKKIKGCWDSIHVVEVQEKSSGRTAHYKLTSTVMLWLQTNKTGSGTMNLGGSLTRQMEKDETVSDSSPHIANIGRLVEDMENKIRSTLNEIYFGKTKDIVNGLRSIDAIPDNQKYKQLQRELSQVLTQRQIYIQPDN /	https://www.addgene.org/101137/ and this paper

		MADFEDRVSDEEKVRIAAKFITHAPPGEFNEVFNDVRLLLNNDNLLREGAAHAF AQYNMDQFTPVKIEGYDDQVLITEHGDLGNGRFLDPRNKISFKFDHLRKEASDP QPEDTESALKQWRDACDSALRAYVKDHYPNGFCTVYGKSIDGQQTIIACIESHQ FQPKNFWNGRWRSEWKFTITPPTAQVAAVLKIQVHYYEDGNVQLVSHKDIQDS VQVSSDVQTAKEFIKIIENAENEYQTAISENYQTMSDTTFKALRRQLPVTRTKID WNKILSYKIGKEMQNA	
Sra1	His6-TEV-hSra1 (1-1253, FL). His6 tag removed by TEV cleavage	MSYYHHHHHHDYDIPTTENLYFQGAMAAQVTLEDALSNVDLLEELPLPDQQPC IEPPPSSLLYQPNFNTNFEDRNAFVTGIARYIEQATVHSSMNEMLEEGQEYAVML YTWRSCSRAIPQVKCNEQPNRVEIYEKTVEVLEPEVTKLMNFMYFQRNAIERFC GEVRRLCHAERRKDFVSEAYLITLGKFINMFAVLDELKNMKCSVKNDHSAYKR AAQFLRKMADPQSIQESQNLSMFLANHNKITQSLQQQLEVISGYEELLADIVNLC VDYYENRMYLTPSEKHMLLKVMGFGLYLMDGSVSNIYKLDAKKRINLSKIDKY FKQLQVVPLFGDMQIELARYIKTSAHYEENKSRWTCTSSGSSPQYNICEQMIQIR EDHMRFISELARYSNSEVVTGSGRQEAQKTDAEYRKLFDLALQGLQLLSQWSA HVMEVYSWKLVHPTDKYSNKDCPDSAEEYERATRYNYTSEEKFALVEVIAMIK GLQVLMGRMESVFNHAIRHTVYAALQDFSQVTLREPLRQAIKKKKNVIQSVLQ AIRKTVCDWETGHEPFNDPALRGEKDPKSGFDIKVPRRAVGPSSTQLYMVRTML ESLIADKSGSKKTLRSSLEGPTILDIEKFHRESFFYTHLINFSETLQQCCDLSQLWF REFFLELTMGRRIQFPIEMSMPWILTDHILETKEASMMEYVLYSLDLYNDSAHY ALTRFNKQFLYDEIEAEVNLCFDQFVYKLADQIFAYYKVMAGSLLLDKRLRSEC KNQGATIHLPPSNRYETLLKQRHVQLLGRSIDLNRLITQRVSAAMYKSLELAIGR FESEDLTSIVELDGLLEINRMTHKLLSRYLTLDGFDAMFREANHNVSAPYGRITL HVFWELNYDFLPNYCYNGSTNRFVRTVLPFSQEFQRDKQPNAQPQYLHGSKAL NLAYSSIYGSYRNFVGPPHFQVICRLLGYQGIAVVMEELLKVVKSLLQGTILQYV KTLMEVMPKICRLPRHEYGSPGILEFFHHQLKDIVEYAELKTVCFQNLREVGNAI LFCLLIEQSLSLEEVCDLLHAAPFQNILPRVHVKEGERLDAKMKRLESKYAPLHL VPLIERLGTPQQIAIAREGDLLTKERLCCGLSMFEVILTRIRSFLDDPIWRGPLPSN GVMHVDECVEFHRLWSAMQFVYCIPVGTHEFTVEQCFGDGLHWAGCMIIVLLG QQRRFAVLDFCYHLLKVQKHDGKDEIIKNVPLKKMVERIRKFQILNDEIITILDK YLKSGDGEGTPVEHVRCFQPPIHQSLASS	(Ismail et al., 2009)
Nap1	hNap1 (1-1128, FL)	MSRSVLQPSQQKLAEKLTILNDRGVGMLTRLYNIKKACGDPKAKPSYLIDKNLE SAVKFIVRKFPAVETRNNNQQLAQLQKEKSEILKNLALYYFTFVDVMEFKDHVC ELLNTIDVCQVFFDITVNFDLTKNYLDLIITYTTLMILLSRIEERKAIIGLYNYAHE MTHGASDREYPRLGQMIVDYENPLKKMMEEFVPHSKSLSDALISLQMVYPRRN LSADQWRNAQLLSLISAPSTMLNPAQSDTMPCEYLSLDAMEKWIIFGFILCHGIL NTDATALNLWKLALQSSSCLSLFRDEVFHIHKAAEDLFVNIRGYNKRINDIRECK EAAVSHAGSMHRERRKFLRSALKELATVLSDQPGLLGPKALFVFMALSFARDEII WLLRHADNMPKKSADDFIDKHIAELIFYMEELRAHVRKYGPVMQRYYVQYLSG FDAVVLNELVQNLSVCPEDESIIMSSFVNTMTSLSVKQVEDGEVFDFRGMRLDW FRLQAYTSVSKASLGLADHRELGKMMNTIIFHTKMVDSLVEMLVETSDLSIFCF YSRAFEKMFQQCLELPSQSRYSIAFPLLCTHFMSCTHELCPEERHHIGDRSLSLCN MFLDEMAKQARNLITDICTEQCTLSDQLLPKHCAKTISQAVNKKSKKQTGKKGE PEREKPGVESMRKNRLVVTNLDKLHTALSELCFSINYVPNMVVWEHTFTPREYL TSHLEIRFTKSIVGMTMYNQATQEIAKPSELLTSVRAYMTVLQSIENYVQIDITRV FNNVLLQQTQHLDSHGEPTITSLYTNWYLETLLRQVSNGHIAYFPAMKAFVNLP TENELTFNAEEYSDISEMRSLSELLGPYGMKFLSESLMWHISSQVAELKKLVVEN VDVLTQMRTSFDKPDQMAALFKRLSSVDSVLKRMTIIGVILSFRSLAQEALRDV LSYHIPFLVSSIEDFKDHIPRETDMKVAMNVYELSSAAGLPCEIDPALVVALSSQK SENISPEEEYKIACLLMVFVAVSLPTLASNVMSQYSPAIEGHCNNIHCLAKAINQI AAALFTIHKGSIEDRLKEFLALASSSLLKIGQETDKTTTRNRESVYLLLDMIVQES PFLTMDLLESCFPYVLLRNAYHAVYKQSVTSSA	(Ismail et al., 2009)
WAVE 1-230	MBP-TEV-hWAVE(1) 1-230, MBP tag removed by TEV cleavage	MKIEEGKLVIWINGDKGYNGLAEVGKKFEKDTGIKVTVEHPDKLEEKFPQVAAT GDGPDIIFWAHDRFGGYAQSGLLAEITPDKAFQDKLYPFTWDAVRYNGKLIAYP IAVEALSLIYNKDLLPNPPKTWEEIPALDKELKAKGKSALMFNLQEPYFTWPLIA ADGGYAFKYENGKYDIKDVGVDNAGAKAGLTFLVDLIKNKHMNADTDYSIAE AAFNKGETAMTINGPWAWSNIDTSKVNYGVTVLPTFKGQPSKPFVGVLSAGINA ASPNKELAKEFLENYLLTDEGLEAVNKDKPLGAVALKSYEEELAKDPRIAATME NAQKGEIMPNIPQMSAFWYAVRTAVINAASGRQTVDEALKDAQTNSSSNNNNN NNNNNLGIEGRISEFENLYFQGHMPLVKRNIDPRHLCHTALPRGIKNELECVTNIS LANIIRQLSSLSKYAEDIFGELFNEAHSFSFRVNSLQERVDRLSVSVTQLDPKEEE LSLQDITMRKAFRSSTIQDQQLFDRKTLPIPLQETYDVCEQPPPLNILTPYRDDGK EGLKFYTNPSYFFDLWKEKMLQDTEDKRKEKRKQKQKNLDRPHEPEKVPRAPH DRRREWQKLAQGPELAEDDANLLHKHIEVANG	(Chen et al., 2017)
WAVE1-230VCA	MBP-TEV-hWAVE(1) 1-230 – GGS6 – VCA, MBP tag removed	MKIEEGKLVIWINGDKGYNGLAEVGKKFEKDTGIKVTVEHPDKLEEKFPQVAAT GDGPDIIFWAHDRFGGYAQSGLLAEITPDKAFQDKLYPFTWDAVRYNGKLIAYP IAVEALSLIYNKDLLPNPPKTWEEIPALDKELKAKGKSALMFNLQEPYFTWPLIA ADGGYAFKYENGKYDIKDVGVDNAGAKAGLTFLVDLIKNKHMNADTDYSIAE AAFNKGETAMTINGPWAWSNIDTSKVNYGVTVLPTFKGQPSKPFVGVLSAGINA ASPNKELAKEFLENYLLTDEGLEAVNKDKPLGAVALKSYEEELAKDPRIAATME	(Chen et al., 2017)

	by TEV cleavage	NAQKGEIMPNIPQMSAFWYAVRTAVINAASGRQTVDEALKDAQTNSSSNNNNN NNNNNLGIEGRISEFENLYFQGHMPLVKRNIDPRHLCHTALPRGIKNELECVTNIS LANIIRQLSSLSKYAEDIFGELFNEAHSFSFRVNSLQERVDRLSVSVTQLDPKEEE LSLQDITMRKAFRSSTIQDQQLFDRKTLPIPLQETYDVCEQPPPLNILTPYRDDGK EGLKFYTNPSYFFDLWKEKMLQDTEDKRKEKRKQKQKNLDRPHEPEKVPRAPH DRRREWQKLAQGPELAEDDANLLHKHIEVANGGGSGGSGGSGGSGGSGGSKR HPSTLPVISDARSVLLEAIRKGIQLRKVEEQREQEAKHERIENDVATILSRRIAVE YSDSEDDSEFDEVDWLE	
Abi 1-158	MBP-TEV-hAbi(2) 1-158, MBP tag removed by TEV cleavage	MKIEEGKLVIWINGDKGYNGLAEVGKKFEKDTGIKVTVEHPDKLEEKFPQVAAT GDGPDIIFWAHDRFGGYAQSGLLAEITPDKAFQDKLYPFTWDAVRYNGKLIAYP IAVEALSLIYNKDLLPNPPKTWEEIPALDKELKAKGKSALMFNLQEPYFTWPLIA ADGGYAFKYENGKYDIKDVGVDNAGAKAGLTFLVDLIKNKHMNADTDYSIAE AAFNKGETAMTINGPWAWSNIDTSKVNYGVTVLPTFKGQPSKPFVGVLSAGINA ASPNKELAKEFLENYLLTDEGLEAVNKDKPLGAVALKSYEEELAKDPRIAATME NAQKGEIMPNIPQMSAFWYAVRTAVINAASGRQTVDEALKDAQTNSSSNNNNN NNNNNLGIEGRISEFENLYFQGHMAELQMLLEEEIPGGRRALFDSYTNLERVAD YCENNYIQSADKQRALEETKAYTTQSLASVAYLINTLANNVLQMLDIQASQLRR MESSINHISQTVDIHKEKVARREIGILTTNKNTSRTHKIIAPANLERPVRYIRKPID YTILDDIGHGVKVSTQ	(Ismail et al., 2009)
Abi 1-158-sortase	MBP-TEV-hAbi(2) 1-158-LPGTG, MBP tag removed by TEV cleavage	MKIEEGKLVIWINGDKGYNGLAEVGKKFEKDTGIKVTVEHPDKLEEKFPQVAAT GDGPDIIFWAHDRFGGYAQSGLLAEITPDKAFQDKLYPFTWDAVRYNGKLIAYP IAVEALSLIYNKDLLPNPPKTWEEIPALDKELKAKGKSALMFNLQEPYFTWPLIA ADGGYAFKYENGKYDIKDVGVDNAGAKAGLTFLVDLIKNKHMNADTDYSIAE AAFNKGETAMTINGPWAWSNIDTSKVNYGVTVLPTFKGQPSKPFVGVLSAGINA ASPNKELAKEFLENYLLTDEGLEAVNKDKPLGAVALKSYEEELAKDPRIAATME NAQKGEIMPNIPQMSAFWYAVRTAVINAASGRQTVDEALKDAQTNSSSNNNNN NNNNNLGIEGRISEFENLYFQGHMAELQMLLEEEIPGGRRALFDSYTNLERVAD YCENNYIQSADKQRALEETKAYTTQSLASVAYLINTLANNVLQMLDIQASQLRR MESSINHISQTVDIHKEKVARREIGILTTNKNTSRTHKIIAPANLERPVRYIRKPID YTILDDIGHGVKVSTQGGLPGTGG	This paper
2MBP-Abi	2MBP-Thrombin-StrepII-hAbi(2) 1-158	MKIEEGKLVIWINGDKGYNGLAEVGKKFEKDTGIKVTVEHPDKLEEKFPQVAAT GDGPDIIFWAHDRFGGYAQSGLLAEITPDKAFQDKLYPFTWDAVRYNGKLIAYP IAVEALSLIYNKDLLPNPPKTWEEIPALDKELKAKGKSALMFNLQEPYFTWPLIA ADGGYAFKYENGKYDIKDVGVDNAGAKAGLTFLVDLIKNKHMNADTDYSIAE AAFNKGETAMTINGPWAWSNIDTSKVNYGVTVLPTFKGQPSKPFVGVLSAGINA ASPNKELAKEFLENYLLTDEGLEAVNKDKPLGAVALKSYEEELAKDPRIAATME NAQKGEIMPNIPQMSAFWYAVRTAVINAASGRQTVDEALKDAQTNSSSLEWSH PQFEKAGGMKIEEGKLVIWINGDKGYNGLAEVGKKFEKDTGIKVTVEHPDKLEE KFPQVAATGDGPDIIFWAHDRFGGYAQSGLLAEITPDKAFQDKLYPFTWDAVRY NGKLIAYPIAVEALSLIYNKDLLPNPPKTWEEIPALDKELKAKGKSALMFNLQEP YFTWPLIAADGGYAFKYENGKYDIKDVGVDNAGAKAGLTFLVDLIKNKHMNA DTDYSIAEAAFNKGETAMTINGPWAWSNIDTSKVNYGVTVLPTFKGQPSKPFVG VLSAGINAASPNKELAKEFLENYLLTDEGLEAVNKDKPLGAVALKSYEEELAKD PRIAATMENAQKGEIMPNIPQMSAFWYAVRTAVINAASGRQTVDEALKDAQTN SSSNNNNNNNNNNLGEFLVPRGSWSHPQFEKAGGHMAELQMLLEEEIPGGRRA LFDSYTNLERVADYCENNYIQSADKQRALEETKAYTTQSLASVAYLINTLANNV LQMLDIQASQLRRMESSINHISQTVDIHKEKVARREIGILTTNKNTSRTHKIIAPA NLERPVRYIRKPIDYTILDDIGHGVKVSTQ	This paper
HSPC300	MBP-TEV-hHSPC300, MBP tag removed by TEV cleavage	MKIEEGKLVIWINGDKGYNGLAEVGKKFEKDTGIKVTVEHPDKLEEKFPQVAAT GDGPDIIFWAHDRFGGYAQSGLLAEITPDKAFQDKLYPFTWDAVRYNGKLIAYP IAVEALSLIYNKDLLPNPPKTWEEIPALDKELKAKGKSALMFNLQEPYFTWPLIA ADGGYAFKYENGKYDIKDVGVDNAGAKAGLTFLVDLIKNKHMNADTDYSIAE AAFNKGETAMTINGPWAWSNIDTSKVNYGVTVLPTFKGQPSKPFVGVLSAGINA ASPNKELAKEFLENYLLTDEGLEAVNKDKPLGAVALKSYEEELAKDPRIAATME NAQKGEIMPNIPQMSAFWYAVRTAVINAASGRQTVDEALKDAQTNSSSNNNNN NNNNNLGIEGRISEFENLYFQGHMGAAMAGQEDPVQREIHQDWANREYIEIITSS IKKIADFLNSFDMSCRSRLATLNEKLTALERRIEYIEARVTKGETLT	(Ismail et al., 2009)
2MBP-HSPC300	2MBP-Thrombin-StrepII-hHSPC300	MKIEEGKLVIWINGDKGYNGLAEVGKKFEKDTGIKVTVEHPDKLEEKFPQVAAT GDGPDIIFWAHDRFGGYAQSGLLAEITPDKAFQDKLYPFTWDAVRYNGKLIAYP IAVEALSLIYNKDLLPNPPKTWEEIPALDKELKAKGKSALMFNLQEPYFTWPLIA ADGGYAFKYENGKYDIKDVGVDNAGAKAGLTFLVDLIKNKHMNADTDYSIAE AAFNKGETAMTINGPWAWSNIDTSKVNYGVTVLPTFKGQPSKPFVGVLSAGINA ASPNKELAKEFLENYLLTDEGLEAVNKDKPLGAVALKSYEEELAKDPRIAATME NAQKGEIMPNIPQMSAFWYAVRTAVINAASGRQTVDEALKDAQTNSSSLEWSH PQFEKAGGMKIEEGKLVIWINGDKGYNGLAEVGKKFEKDTGIKVTVEHPDKLEE KFPQVAATGDGPDIIFWAHDRFGGYAQSGLLAEITPDKAFQDKLYPFTWDAVRY NGKLIAYPIAVEALSLIYNKDLLPNPPKTWEEIPALDKELKAKGKSALMFNLQEP YFTWPLIAADGGYAFKYENGKYDIKDVGVDNAGAKAGLTFLVDLIKNKHMNA DTDYSIAEAAFNKGETAMTINGPWAWSNIDTSKVNYGVTVLPTFKGQPSKPFVG VLSAGINAASPNKELAKEFLENYLLTDEGLEAVNKDKPLGAVALKSYEEELAKD	(Chen et al., 2014)

		PRIAATMENAQKGEIMPNIPQMSAFWYAVRTAVINAASGRQTVDEALKDAQTN SSSNNNNNNNNNNLGEFLVPRGSWSHPQFEKAGGHMGAAMAGQEDPVQREIH QDWANREYIEIITSSIKKIADFLNSFDMSCRSRLATLNEKLTALERRIEYIEARVTK GETLT	
GG-2MBP	MKI-GGS-TEV-GG-2MBP-TEV, N-terminal and C-terminal regions removed after TEV cleavage	MKIGGSENLYFQGGGKTEEGKLVIWINGDKGYNGLAEVGKKFEKDTGIKVTVE HPDKLEEKFPQVAATGDGPDIIFWAHDRFGGYAQSGLLAEITPDKAFQDKLYPF TWDAVRYNGKLIAYPIAVEALSLIYNKDLLPNPPKTWEEIPALDKELKAKGKSA LMFNLQEPYFTWPLIAADGGYAFKYENGKYDIKDVGVDNAGAKAGLTFLVDLI KNKHMNADTDYSIAEAAFNKGETAMTINGPWAWSNIDTSKVNYGVTVLPTFKG QPSKPFVGVLSAGINAASPNKELAKEFLENYLLTDEGLEAVNKDKPLGAVALKS YEEELAKDPRIAATMENAQKGEIMPNIPQMSAFWYAVRTAVINAASGRQTVDE ALKDAQTNSSSNNGGSGGSGGSKTEEGKLVIWINGDKGYNGLAEVGKKFEKDT GIKVTVEHPDKLEEKFPQVAATGDGPDIIFWAHDRFGGYAQSGLLAEITPDKAFQ DKLYPFTWDAVRYNGKLIAYPIAVEALSLIYNKDLLPNPPKTWEEIPALDKELKA KGKSALMFNLQEPYFTWPLIAADGGYAFKYENGKYDIKDVGVDNAGAKAGLT FLVDLIKNKHMNADTDYSIAEAAFNKGETAMTINGPWAWSNIDTSKVNYGVTV LPTFKGQPSKPFVGVLSAGINAASPNKELAKEFLENYLLTDEGLEAVNKDKPLG AVALKSYEEELAKDPRIAATMENAQKGEIMPNIPQMSAFWYAVRTAVINAASG RQTVDEALKDAQTNSSSNNNNNNNNNNLGIEGRISEFENLYFQGHMLEEFGSSR VDLQASLALAVVLQRRDWENPGVTQLNRLAAHPPFASWRNSEEARTDRPSQQL RSLNGEWQLGCFGG	This paper
Sortase 5M	Sortase 5M-His6	MQAKPQIPKDKSKVAGYIEIPDADIKEPVYPGPATREQLNRGVSFAEENESLDDQ NISIAGHTFIDRPNYQFTNLKAAKKGSMVYFKVGNETRKYKMTSIRNVKPTAVE VLDEQKGKDKQLTLITCDDYNEETGVWETRKIFVATEVKLEHHHHHH	https://www.addgene.org/75144/
Rac QP	hRac Q61L/P29SΔ4	MQAIKCVVVGDGAVGKTCLLISYTTNAFSGEYIPTVFDNYSANVMVDGKPVNL GLWDTAGLEDYDRLRPLSYPQTDVFLICFSLVSPASFENVRAKWYPEVRHHCPN TPIILVGTKLDLRDDKDTIEKLKEKKLTPITYPQGLAMAKEIGAVKYLECSALTQ RGLKTVFDEAIRAVLCPPPVKKRKRKCLLL	This paper

792

793

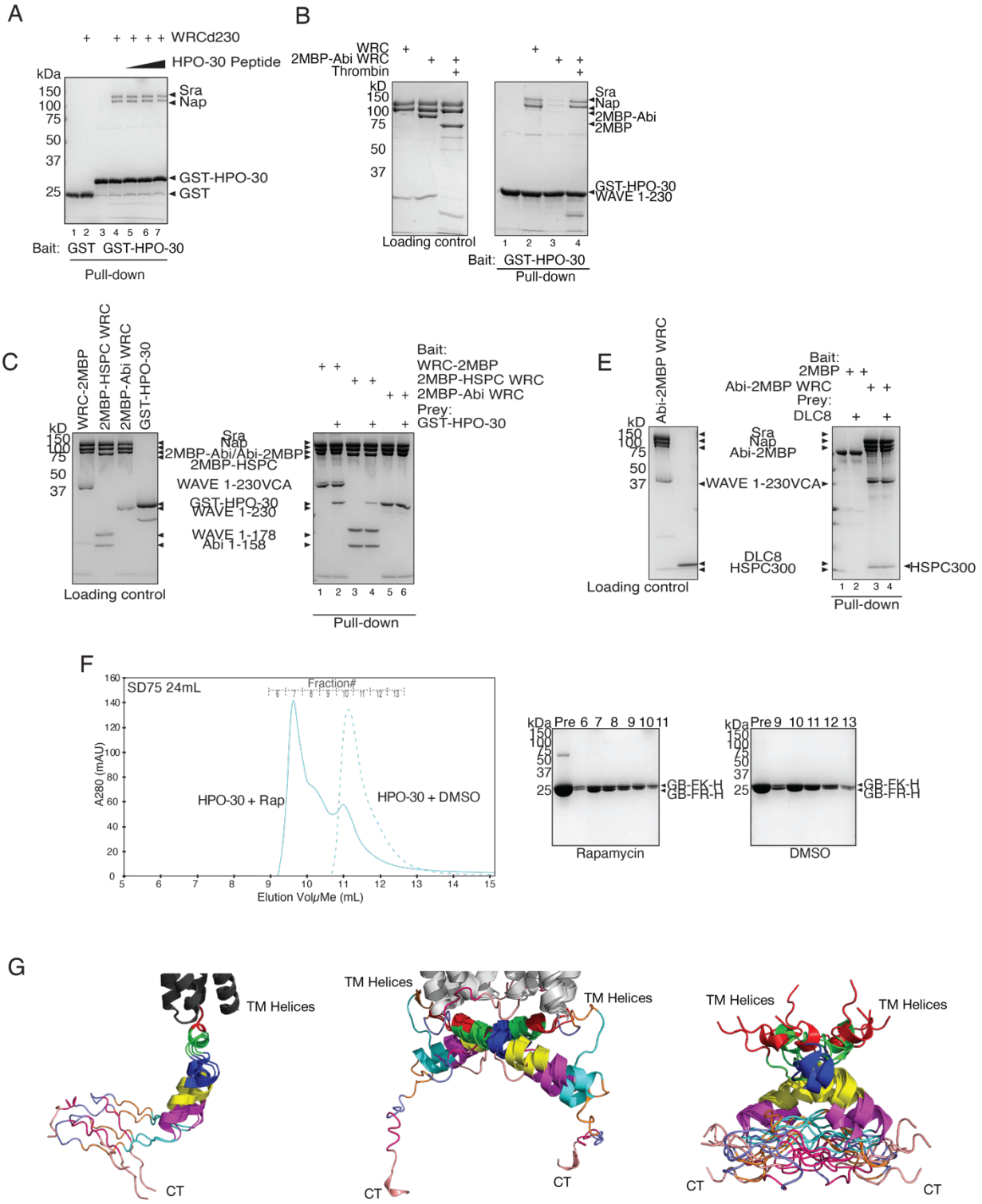

794

795 **Supplemental Figure 1. HPO-30 ICD binding to WRC is enhanced by dimerization.** A)

796 Immobilized GST-HPO30 pulling down WRC, with HPO-30 peptide added as a competitor.

797 Bait: 200 pmol, Prey: 150 pmol, Competitor: 18000-100000 pmol, 50 mM NaCl. B)
798 Immobilized $(MBP)_2$-Abi2 WRC pulling down GST-HPO-30, with and without thrombin to
799 cleave off the $(MBP)_2$ tag. Bait: 200 pmol, Prey: 150 pmol, thrombin added overnight, 50 mM
800 NaCl. C) Immobilized WRC-$(MBP)_2$, $(MBP)_2$-HSPC300 WRC, and $(MBP)_2$-Abi2 WRC pulling
801 down GST-HPO-30. Bait: 60 pmol, Prey: 600 pmol, 50 mM NaCl. D) Immobilized $(MBP)_2$ or
802 WRC-$(MBP)_2$ pulling down empty DLC8 vector. Bait: 60 pmol, Prey: 600 pmol, 50 mM NaCl.
803 E) Left, gel filtration profiles of equimolar GB1-FKBP-HPO30 and GB1-FRB-HPO30, with and
804 without rapamycin. 5 μM rapamycin or equivalent volume of DMSO, 100 mM NaCl. Right,
805 Coomassie-stained SDS-PAGE gels of the fractions. F) Right, AlphaFold 2.0 structures of the
806 monomeric HPO-30 ICD in the context of full-length protein (same as Figure 1G, left). Middle,
807 AlphaFold 2.0 structures of the dimeric HPO-30 ICD in the context of full-length protein. Right,
808 AlphaFold 2.0 structures of the dimeric HPO-30 ICD in the context of just the ICD.
809

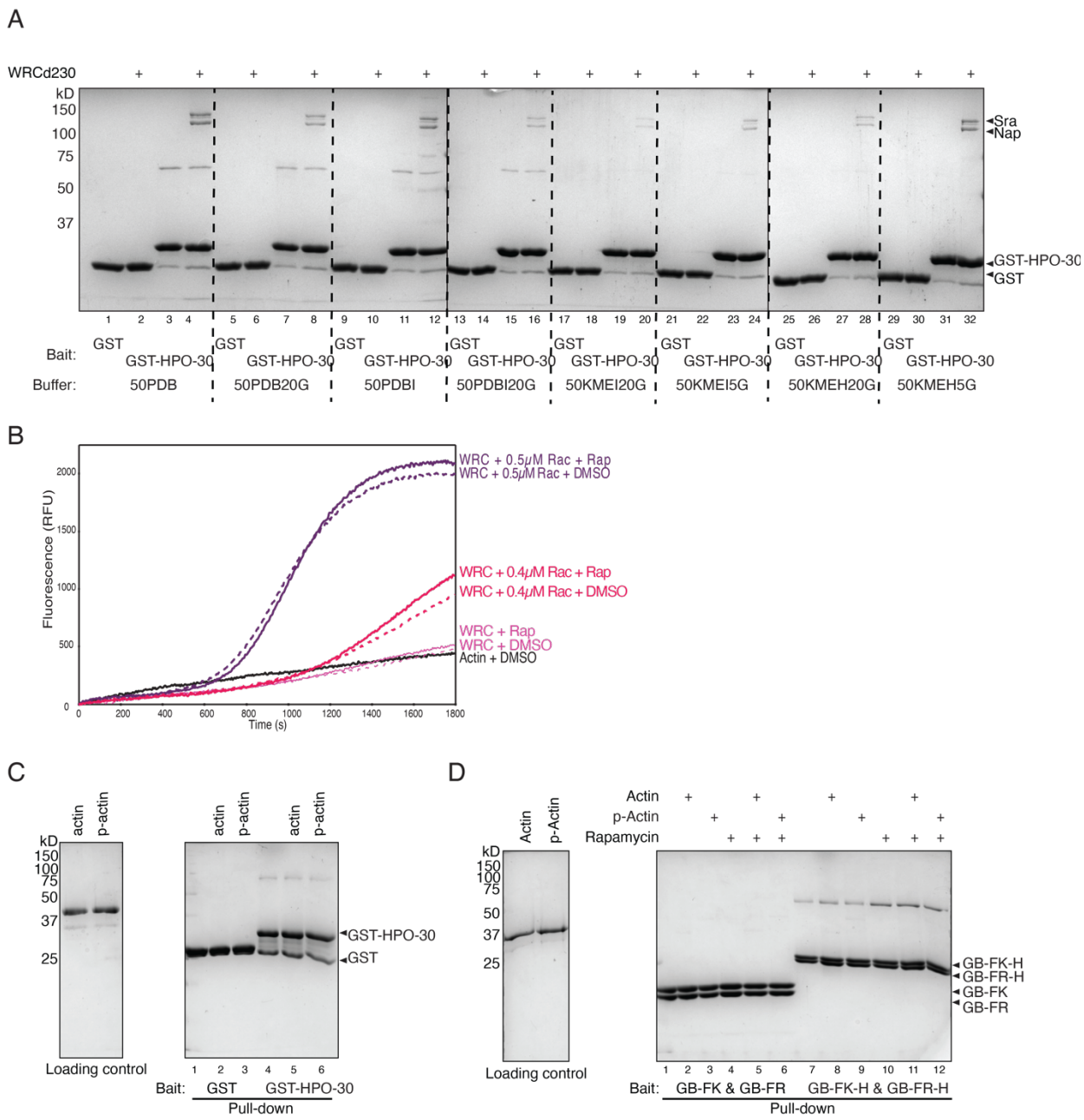

Supplemental Figure 2. HPO-30 ICD may act as an actin capping protein. A) Immobilized GST-HPO-30 pulling down WRC in various buffers. Abbreviations: 50PDB, pull down buffer, 50 mM NaCl, 10 mM HEPES pH 7.0, 5% glycerol; 20 G, 20% glycerol; I, 10 mM Imidazole pH 7.0; 50KMEI20G, 50 mM KCl, 2 mM $MgCl_2$, 1 mM EGTA pH 8.0, 10 mM Imidazole pH 7.0, 20% glycerol; 5G, 5% glycerol. Bait: 200 pmol, Prey:150 pmol. B) Actin polymerization assays

816 using 4 μM actin/20% pyrene-labeling, 10 nM Arp2/3 complex, 100 nM WRC230VCA, and 0.4
817 μM or 0.5 μM Rac2 QP. 5 μM rapamycin (solid curves) or equivalent volume of DMSO (dashed
818 curves) added. C) Immobilized GST-HPO-30 pulling down actin or pyrene labeled actin (p-
819 actin). Bait: 200 pmol, prey: 500 pmol, 2 mM Tris-HCl pH 8, 0.5 mM DTT, 0.2 mM ATP, 0.1
820 mM $CaCl_2$, 1 mM NaN3. D) Immobilized equimolar GB1-FKBP-HPO-30/GB1-FRB-HPO-30
821 pulling down actin and p-actin. Bait: 300 pmol, Prey: 300 pmol, 2 mM Tris-HCl pH 8.0, 0.5 mM
822 DTT, 0.2 mM ATP, 0.1 mM $CaCl_2$, 1 mM NaN_3. 5 μM rapamycin or equivalent volume of
823 DMSO was added.
824

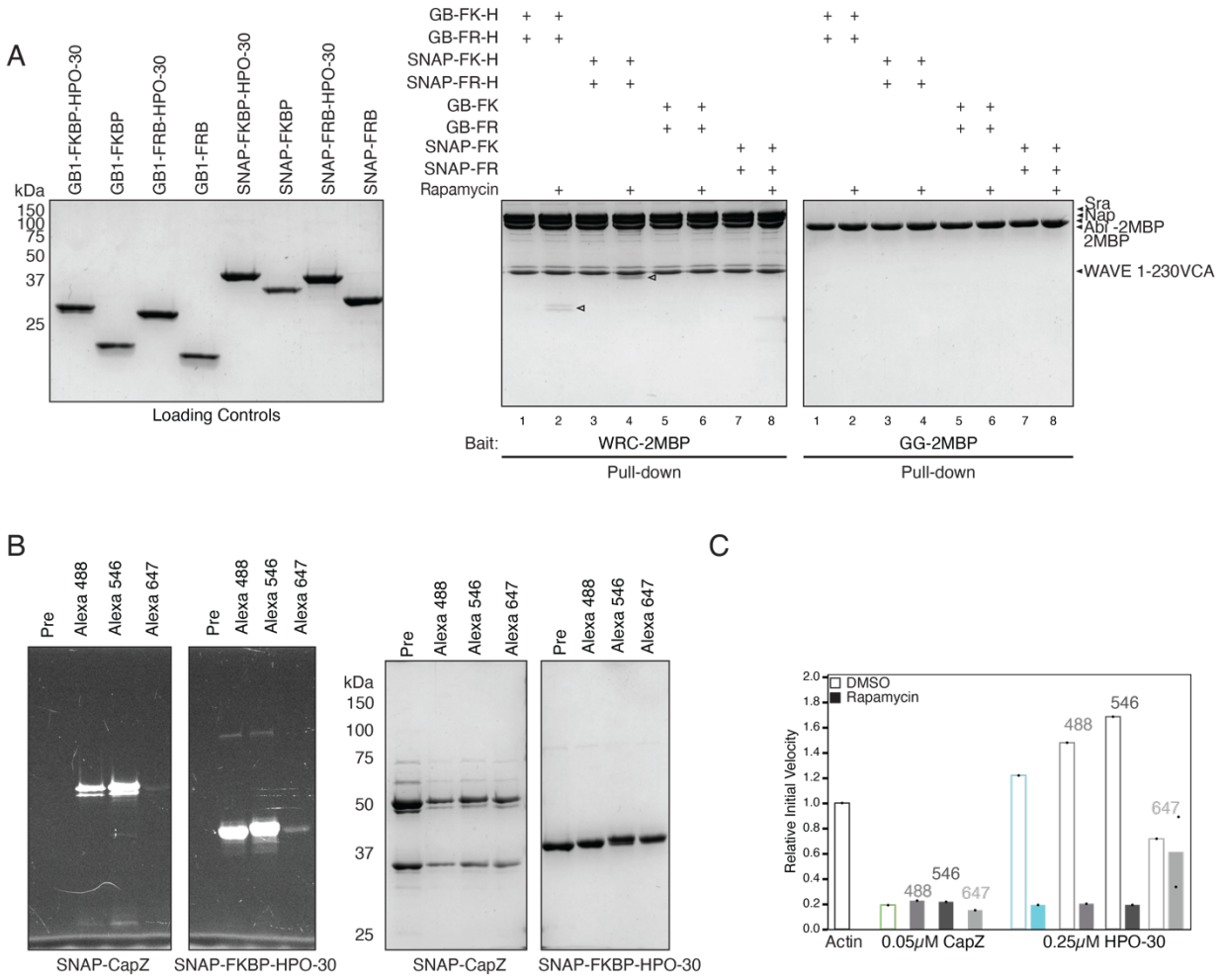

825

826 **Supplemental Figure 3. HPO-30 ICD inhibits actin polymerization and depolymerization.**

827 A) Immobilized WRC-2MBP pulling down GB1-tagged and SNAP-tagged HPO-30 constructs.

828 Abbreviations are as used before. Bait: 60 pmol, Prey: 600 pmol, 50 mM NaCl, 10 mM HEPES

829 pH 7.0, 5% glycerol. B) SNAP-tag labeling of CapZ, FKBP-HPO-30, and FKBP with SNAP-

830 Surface© AlexaFluor©-488 (Alexa 488), SNAP-Surface© AlexaFluor©-546 (Alexa 546), and

831 SNAP-Surface© AlexaFluor©-647 (Alexa 647). Left, SDS-PAGE gel visualized with Alexa-488

832 filter. Right, Coomassie blue-stained SDS-PAGE gel. C) Actin depolymerization assays using

833 SNAP-Alexa labeled proteins. 5 μM actin diluted 20-fold with 25% 50KMEH5Gd/75%GMg. 5

834 μM rapamycin or equivalent volume of DMSO added. Labeled proteins are denoted by the

835 number associated with the dye they are labeled with. Colored bars represent wild type protein.

836

837 **References**

838 Akin, O., Mullins, R.D., 2008. Capping Protein Increases the Rate of Actin-Based Motility by
839 Promoting Filament Nucleation by the Arp2/3 Complex. Cell 133, 841–851.
840 https://doi.org/10.1016/j.cell.2008.04.011

841 Alekhina, O., Burstein, E., Billadeau, D.D., 2017. Cellular functions of WASP family proteins at
842 a glance. J. Cell Sci. 130, 2235–2241. https://doi.org/10.1242/jcs.199570

843 Banaszynski, L.A., Liu, C.W., Wandless, T.J., 2005. Characterization of the
844 FKBP·Rapamycin·FRB Ternary Complex. J. Am. Chem. Soc. 127, 4715–4721.
845 https://doi.org/10.1021/ja043277y

846 Begemann, A., Sticht, H., Begtrup, A., Vitobello, A., Faivre, L., Banka, S., Alhaddad, B.,
847 Asadollahi, R., Becker, J., Bierhals, T., Brown, K.E., Bruel, A.L., Brunet, T., Carneiro, M.,
848 Cremer, K., Day, R., Denommé-Pichon, A.S., Dyment, D.A., Engels, H., Fisher, R., Goh,
849 E.S., Hajianpour, M.J., Haertel, L.R.M., Hauer, N., Hempel, M., Herget, T., Johannsen, J.,
850 Kraus, C., Le Guyader, G., Lesca, G., Mau-Them, F.T., McDermott, J.H., McWalter, K.,
851 Meyer, P., Õunap, K., Popp, B., Reimand, T., Riedhammer, K.M., Russo, M., Sadleir, L.G.,
852 Saenz, M., Schiff, M., Schuler, E., Syrbe, S., Van der Ven, A.T., Verloes, A., Willems, M.,
853 Zweier, C., Steindl, K., Zweier, M., Rauch, A., 2021. New insights into the clinical and
854 molecular spectrum of the novel CYFIP2-related neurodevelopmental disorder and
855 impairment of the WRC-mediated actin dynamics. Genet. Med. 23, 543–554.
856 https://doi.org/10.1038/s41436-020-01011-x

857 Burianek, L.E., Soderling, S.H., 2013. Under lock and key: Spatiotemporal regulation of WASP
858 family proteins coordinates separate dynamic cellular processes. Semin. Cell Dev. Biol. 24,
859 258–266. https://doi.org/10.1016/j.semcdb.2012.12.005

860 Caldwell, J.E., Heiss, S.G., Mermall, V., Cooper, J.A., 1989. Effects of CapZ, an Actin Capping
861 Protein of Muscle, on the Polymerization of Actin. Biochemistry 28, 8506–8514.
862 https://doi.org/10.1021/bi00447a036
863 Chaudhari, K., Gorla, M., Chang, C., Kania, A., Bashaw, G.J., 2021. Robo recruitment of the
864 wave regulatory complex plays an essential and conserved role in midline repulsion. Elife
865 10, 1–35. https://doi.org/10.7554/ELIFE.64474
866 Chen, B., Brinkmann, K., Chen, Z., Pak, C.W., Liao, Y., Shi, S., Henry, L., Grishin, N. V.,
867 Bogdan, S., Rosen, M.K., 2014a. The WAVE regulatory complex links diverse receptors to
868 the actin cytoskeleton. Cell 156, 195–207. https://doi.org/10.1016/j.cell.2013.11.048
869 Chen, B., Brinkmann, K., Chen, Z., Pak, C.W., Liao, Y., Shi, S., Henry, L., Grishin, N. V.,
870 Bogdan, S., Rosen, M.K., 2014b. The WAVE regulatory complex links diverse receptors to
871 the actin cytoskeleton. Cell 156, 195–207. https://doi.org/10.1016/j.cell.2013.11.048
872 Chen, B., Chou, H.-T., Brautigam, C.A., Xing, W., Yang, S., Henry, L., Doolittle, L.K., Walz,
873 T., Rosen, M.K., 2017a. Rac1 GTPase activates the WAVE regulatory complex through
874 two distinct binding sites. Elife 6, 1–22. https://doi.org/10.7554/elife.29795
875 Chen, B., Chou, H.-T., Brautigam, C.A., Xing, W., Yang, S., Henry, L., Doolittle, L.K., Walz,
876 T., Rosen, M.K., 2017b. Rac1 GTPase activates the WAVE regulatory complex through
877 two distinct binding sites. Elife 6. https://doi.org/10.7554/elife.29795
878 Chen, B., Padrick, S.B., Henry, L., Rosen, M.K., 2014c. Biochemical reconstitution of the
879 WAVE regulatory complex. Methods Enzymol. 540, 55–72. https://doi.org/10.1016/B978-
880 0-12-397924-7.00004-2
881 Chen, I., Dorr, B.M., Liu, D.R., 2011. A general strategy for the evolution of bond-forming
882 enzymes using yeast display. Proc. Natl. Acad. Sci. U. S. A. 108, 11399–11404.

883 https://doi.org/10.1073/pnas.1101046108

884 Chen, Z., Borek, D., Padrick, S.B., Gomez, T.S., Metlagel, Z., Ismail, A.M., Umetani, J.,
885 Billadeau, D.D., Otwinowski, Z., Rosen, M.K., 2010a. Structure and control of the actin
886 regulatory WAVE complex. Nature 468, 533–538. https://doi.org/10.1038/nature09623

887 Chen, Z., Borek, D., Padrick, S.B., Gomez, T.S., Metlagel, Z., Ismail, A.M., Umetani, J.,
888 Billadeau, D.D., Otwinowski, Z., Rosen, M.K., 2010b. Structure and control of the actin
889 regulatory WAVE complex. Nature 468, 533–538. https://doi.org/10.1038/nature09623

890 Cheng, P., Poo, M., 2012. Early events in axon/dendrite polarization. Annu. Rev. Neurosci. 35,
891 181–201. https://doi.org/10.1146/annurev-neuro-061010-113618

892 Chia, P.H., Chen, B., Li, P., Rosen, M.K., Shen, K., 2014. Local F-actin network links synapse
893 formation and axon branching. Cell 156, 208–220.
894 https://doi.org/10.1016/j.cell.2013.12.009

895 Conway, O.J., Carrasquillo, M.M., Wang, X., Bredenberg, J.M., Reddy, J.S., Strickland, S.L.,
896 Younkin, C.S., Burgess, J.D., Allen, M., Lincoln, S.J., Nguyen, T., Malphrus, K.G., Soto,
897 A.I., Walton, R.L., Boeve, B.F., Petersen, R.C., Lucas, J.A., Ferman, T.J., Cheshire, W.P.,
898 van Gerpen, J.A., Uitti, R.J., Wszolek, Z.K., Ross, O.A., Dickson, D.W., Graff-Radford,
899 N.R., Ertekin-Taner, N., 2018. ABI3 and PLCG2 missense variants as risk factors for
900 neurodegenerative diseases in Caucasians and African Americans. Mol. Neurodegener. 13,
901 1–12. https://doi.org/10.1186/s13024-018-0289-x

902 Cooper, J.A., Pollard, T.D., 1985. Effects of Capping Protein on the Kinetics of Actin
903 Polymerization. Biochemistry 793–799.

904 Cooper, J.A., Walker, S.B., Pollard, T.D., 1983. Pyrene actin: documentation of the validity of a
905 sensitive assay for actin polymerization. J. Muscle Res. Cell Motil. 4, 253–262.

906 https://doi.org/10.1007/BF00712034

907 Dahl, J.P., Wang-Dunlop, J., Gonzales, C., Goad, M.E.P., Mark, R.J., Kwak, S.P., 2003.
908 Characterization of the WAVE1 knock-out mouse: Implications for CNS development. J.
909 Neurosci. 23, 3343–3352. https://doi.org/10.1523/jneurosci.23-08-03343.2003

910 Dong, X., Liu, O.W., Howell, A.S., Shen, K., 2013. An extracellular adhesion molecule complex
911 patterns dendritic branching and morphogenesis. Cell 155, 296.
912 https://doi.org/10.1016/j.cell.2013.08.059

913 Doolittle, L.K., Rosen, M.K., Padrick, S.B., 2013a. Measurement and analysis of in vitro actin
914 polymerization. Methods Mol. Biol. 1046, 273–293. https://doi.org/10.1007/978-1-62703-
915 538-5_16

916 Doolittle, L.K., Rosen, M.K., Padrick, S.B., 2013b. Purification of native Arp2/3 complex from
917 bovine thymus. Methods Mol. Biol. 1046, 231–250. https://doi.org/10.1007/978-1-62703-
918 538-5_14

919 Dyson, H.J., Wright, P.E., 2002. Coupling of folding and binding for unstructured proteins. Curr.
920 Opin. Struct. Biol. 12, 54–60. https://doi.org/10.1016/S0959-440X(02)00289-0

921 Eden, S., Rohatgi, R., Podtelejnikov, A. V., Mann, M., Kirschner, M.W., 2002. Mechanism of
922 regulation of WAVE1-induced actin nucleation by Rac1 and Nck. Nature 418, 790–793.
923 https://doi.org/10.1038/nature00859

924 Fan, L., Lu, Y., Shen, X., Shao, H., Suo, L., Wu, Q., 2018. Alpha protocadherins and Pyk2
925 kinase regulate cortical neuron migration and cytoskeletal dynamics via rac1 GTPase and
926 WAVE complex in mice. Elife 7, 1–26. https://doi.org/10.7554/eLife.35242

927 Gautreau, A., Ho, H. -y. H., Li, J., Steen, H., Gygi, S.P., Kirschner, M.W., 2004. Purification and
928 architecture of the ubiquitous Wave complex. Proc. Natl. Acad. Sci. 101, 4379–4383.

929 https://doi.org/10.1073/pnas.0400628101
930 Goley, E.D., Welch, M.D., 2006. The ARP2/3 complex: An actin nucleator comes of age. Nat.
931 Rev. Mol. Cell Biol. 7, 713–726. https://doi.org/10.1038/nrm2026
932 Greenfield, N.J., 2006. Using circular dichroism spectra to estimate protein secondary structure.
933 Nat. Protoc. 1, 2876–2890. https://doi.org/10.1038/nprot.2006.202
934 Heier, J.A., Dickinson, D.J., Kwiatkowski, A. V, 2017. Measuring Protein Binding to F-actin by
935 Co-sedimentation. J. Vis. Exp. 55613. https://doi.org/10.3791/55613
936 Heiss, S.G., Cooper, J.A., 1991. Regulation of CapZ, an Actin Capping Protein of Chicken
937 Muscle, by Anionic Phospholipids. Biochemistry 30, 8753–8758.
938 https://doi.org/10.1021/bi00100a006
939 Hotulainen, P., Hoogenraad, C.C., 2010. Actin in dendritic spines: Connecting dynamics to
940 function. J. Cell Biol. 189, 619–629. https://doi.org/10.1083/jcb.201003008
941 Huxley, H.E., Brown, W., 1967. The low-angle X-ray diagram of vertebrate striated muscle and
942 its behaviour during contraction and rigor. J. Mol. Biol. 30, 383–434.
943 https://doi.org/10.1016/S0022-2836(67)80046-9
944 Ito, Y., Carss, K.J., Duarte, S.T., Hartley, T., Keren, B., Kurian, M.A., Marey, I., Charles, P.,
945 Mendonça, C., Nava, C., Pfundt, R., Sanchis-Juan, A., van Bokhoven, H., van Essen, A.,
946 van Ravenswaaij-Arts, C., Aitman, T., Bennett, D., Caulfield, M., Chinnery, P., Gale, D.,
947 Koziell, A., Kuijpers, T.W., Laffan, M.A., Maher, E., Markus, H.S., Morrell, N.W.,
948 Ouwehand, W.H., Perry, D.J., Raymond, F.L., Roberts, I., Smith, K.G.C., Thrasher, A.,
949 Watkins, H., Williamson, C., Woods, G., Ashford, S., Bradley, J.R., Fletcher, D.,
950 Hammerton, T., James, R., Kingston, N., Penkett, C.J., Stirrups, K., Veltman, M., Young,
951 T., Brown, M., Clements-Brod, N., Davis, J., Dewhurst, E., Dolling, H., Erwood, M., Frary,

A., Linger, R., Martin, J.M., Papadia, S., Rehnstrom, K., Stark, H., Allsup, D., Austin, S., Bakchoul, T., Bariana, T.K., Bolton-Maggs, P., Chalmers, E., Collins, J., Collins, P., Erber, W.N., Everington, T., Favier, R., Freson, K., Furie, B., Gattens, M., Gebhart, J., Gomez, K., Greene, D., Greinacher, A., Gresele, P., Hart, D., Heemskerk, J.W.M., Henskens, Y., Kazmi, R., Keeling, D., Kelly, A.M., Lambert, M.P., Lentaigne, C., Liesner, R., Makris, M., Mangles, S., Mathias, M., Millar, C.M., Mumford, A., Nurden, P., Payne, J., Pasi, J., Peerlinck, K., Revel-Vilk, S., Richards, M., Rondina, M., Roughley, C., Schulman, S., Schulze, H., Scully, M., Sivapalaratnam, S., Stubbs, M., Tait, R.C., Talks, K., Thachil, J., Toh, C.H., Turro, E., Van Geet, C., De Vries, M., Warner, T.Q., Watson, H., Westbury, S., Furnell, A., Mapeta, R., Rayner-Matthews, P., Simeoni, I., Staines, S., Stephens, J., Watt, C., Whitehorn, D., Attwood, A., Daugherty, L., Deevi, S.V.V., Halmagyi, C., Hu, F., Matser, V., Meacham, S., Megy, K., Shamardina, O., Titterton, C., Tuna, S., Yu, P., von Ziegenweldt, J., Astle, W., Bleda, M., Carss, K.J., Gräf, S., Haimel, M., Lango-Allen, H., Richardson, S., Calleja, P., Rankin, S., Turek, W., Anderson, J., Bryson, C., Carmichael, J., McJannet, C., Stock, S., Allen, L., Ambegaonkar, G., Armstrong, R., Arno, G., Bitner-Glindzicz, M., Brady, A., Canham, N., Chitre, M., Clement, E., Clowes, V., Deegan, P., Deshpande, C., Doffinger, R., Firth, H., Flinter, F., French, C., Gardham, A., Ghali, N., Gissen, P., Grozeva, D., Henderson, R., Hensiek, A., Holden, S., Holder, M., Holder, S., Hurst, J., Josifova, D., Krishnakumar, D., Kurian, M.A., Lees, M., MacLaren, R., Maw, A., Mehta, S., Michaelides, M., Moore, A., Murphy, E., Park, S.M., Parker, A., Patch, C., Paterson, J., Rankin, J., Reid, E., Rosser, E., Sanchis-Juan, A., Sandford, R., Santra, S., Scott, R., Sohal, A., Stein, P., Thomas, E., Thompson, D., Tischkowitz, M., Vogt, J., Wakeling, E., Wassmer, E., Webster, A., Ali, Sonia, Ali, Souad, Boggard, H.J., Church, C.,

975 Coghlan, G., Cookson, V., Corris, P.A., Creaser-Myers, A., DaCosta, R., Dormand, N.,
976 Eyries, M., Gall, H., Ghataorhe, P.K., Ghio, S., Ghofrani, A., Gibbs, J.S.R., Girerd, B.,
977 Greenhalgh, A., Hadinnapola, C., Houweling, A.C., Humbert, M., in't Veld, A.H.,
978 Kennedy, F., Kiely, D.G., Kovacs, G., Lawrie, A., Ross, R.V.M., Machado, R., Masati, L.,
979 Meehan, S., Moledina, S., Montani, D., Othman, S., Peacock, A.J., Pepke-Zaba, J., Pollock,
980 V., Polwarth, G., Ranganathan, L., Rhodes, C.J., Rue-Albrecht, K., Schotte, G., Shipley, D.,
981 Soubrier, F., Southgate, L., Scelsi, L., Suntharalingam, J., Tan, Y., Toshner, M., Treacy,
982 C.M., Trembath, R., Noordegraaf, A.V., Walker, Sara, Wanjiku, I., Wharton, J., Wilkins,
983 M., Wort, S.J., Yates, K., Alachkar, H., Antrobus, R., Arumugakani, G., Bacchelli, C.,
984 Baxendale, H., Bethune, C., Bibi, S., Booth, C., Browning, M., Burns, S., Chandra, A.,
985 Cooper, N., Davies, S., Devlin, L., Drewe, E., Edgar, D., Egner, W., Ghurye, R., Gilmour,
986 K., Goddard, S., Gordins, P., Grigoriadou, S., Hackett, S., Hague, R., Harper, L., Hayman,
987 G., Herwadkar, A., Huissoon, A., Jolles, S., Kelleher, P., Kumararatne, D., Lear, S.,
988 Longhurst, H., Lorenzo, L., Maimaris, J., Manson, A., McDermott, E., Murng, S.,
989 Nejentsev, S., Noorani, S., Oksenhendler, E., Ponsford, M., Qasim, W., Quinti, I., Richter,
990 A., Samarghitean, C., Sargur, R., Savic, S., Seneviratne, S., Sewell, C., Staples, E., Stauss,
991 H., Thaventhiran, J., Thomas, M., Welch, S., Willcocks, L., Yeatman, N., Yong, P., Ancliff,
992 P., Babbs, C., Layton, M., Louka, E., McGowan, S., Mead, A., Roy, N., Chambers, J.,
993 Dixon, P., Estiu, C., Hague, B., Marschall, H.U., Simpson, M., Chong, S., Emmerson, I.,
994 Ginsberg, L., Gosal, D., Hadden, R., Horvath, R., Mahdi-Rogers, M., Manzur, A., Marshall,
995 A., Matthews, E., McCarthy, M., Reilly, M., Renton, T., Rice, A., Themistocleous, A.,
996 Vale, T., Van Zuydam, N., Walker, Suellen, Ormondroyd, L., Hudson, G., Wei, W., Yu
997 Wai Man, P., Whitworth, J., Afzal, M., Colby, E., Saleem, M., Alavijeh, O.S., Cook, H.T.,

998 Johnson, S., Levine, A.P., Wong, E.K.S., Tan, R., Boycott, K.M., MacKenzie, A.,
999 Majewski, J., Brudno, M., Bulman, D., Dyment, D., Boycott, K.M., Kernohan, K.D.,
1000 Dyack, S., Raymond, F.L., 2018. De Novo Truncating Mutations in WASF1 Cause
1001 Intellectual Disability with Seizures. Am. J. Hum. Genet. 103, 144–153.
1002 https://doi.org/10.1016/j.ajhg.2018.06.001
1003 Jan, Y.-N., Jan, L.Y., 2003. The Control of Dendrite Development. Neuron 40, 229–242.
1004 https://doi.org/https://doi.org/10.1016/S0896-6273(03)00631-7
1005 Jumper, J., Evans, R., Pritzel, A., Green, T., Figurnov, M., Ronneberger, O., Tunyasuvunakool,
1006 K., Bates, R., Žídek, A., Potapenko, A., Bridgland, A., Meyer, C., Kohl, S.A.A., Ballard,
1007 A.J., Cowie, A., Romera-Paredes, B., Nikolov, S., Jain, R., Adler, J., Back, T., Petersen, S.,
1008 Reiman, D., Clancy, E., Zielinski, M., Steinegger, M., Pacholska, M., Berghammer, T.,
1009 Bodenstein, S., Silver, D., Vinyals, O., Senior, A.W., Kavukcuoglu, K., Kohli, P., Hassabis,
1010 D., 2021. Highly accurate protein structure prediction with AlphaFold. Nature 596, 583–
1011 589. https://doi.org/10.1038/s41586-021-03819-2
1012 Kirkpatrick, S.L., Goldberg, L.R., Yazdani, N., Babbs, R.K., Wu, J., Reed, E.R., Jenkins, D.F.,
1013 Bolgioni, A.F., Landaverde, K.I., Luttik, K.P., Mitchell, K.S., Kumar, V., Johnson, W.E.,
1014 Mulligan, M.K., Cottone, P., Bryant, C.D., 2017. Cytoplasmic FMR1-Interacting Protein 2
1015 Is a Major Genetic Factor Underlying Binge Eating. Biol. Psychiatry 81, 757–769.
1016 https://doi.org/10.1016/j.biopsych.2016.10.021
1017 Kobayashi, K., Kuroda, S., Fukata, M., Nakamura, T., Nagase, T., Nomura, N., Matsuura, Y.,
1018 Yoshida-Kubomura, N., Iwamatsu, A., Kaibuchi, K., 1998. p140Sra-1 (specifically Rac1-
1019 associated protein) is a novel specific target for Rac1 small GTPase. J. Biol. Chem. 273,
1020 291–295. https://doi.org/10.1074/jbc.273.1.291

1021 Koronakis, V., Hume, P.J., Humphreys, D., Liu, T., Horning, O., Jensen, O.N., McGhie, E.J.,
1022 2011. WAVE regulatory complex activation by cooperating GTPases Arf and Rac1. Proc.
1023 Natl. Acad. Sci. 108, 14449–14454. https://doi.org/10.1073/pnas.1107666108
1024 Kouyama, T., Mihashi, K., 1981. Fluorimetry study of N-(1-pyrenyl)iodoacetamide-labelled F-
1025 actin. Local structural change of actin protomer both on polymerization and on binding of
1026 heavy meromyosin. Eur. J. Biochem. 114, 33–38.
1027 Kuhn, J.R., Pollard, T.D., 2005. Real-time measurements of actin filament polymerization by
1028 total internal reflection fluorescence microscopy. Biophys. J. 88, 1387–1402.
1029 https://doi.org/10.1529/biophysj.104.047399
1030 Kumar, V., Kim, K., Joseph, C., Kourrich, S., Yoo, S.-H., Huang, H.C., Vitaterna, M.H., de
1031 Villena, F.P.-M., Churchill, G., Bonci, A., Takahashi, J.S., 2013. C57BL/6N Mutation in
1032 Cytoplasmic FMRP interacting protein 2 Regulates Cocaine Response. Science (80-.). 342,
1033 1508–1512.
1034 Kuzmic, P., 1996. Program DYNAFIT for the analysis of enzyme kinetic data: application to
1035 HIV proteinase. Anal. Biochem. 237, 260–273. https://doi.org/10.1006/abio.1996.0238
1036 Lebensohn, A.M., Kirschner, M.W., 2009. Activation of the WAVE Complex by Coincident
1037 Signals Controls Actin Assembly. Mol. Cell 36, 512–524.
1038 https://doi.org/10.1016/j.molcel.2009.10.024
1039 Lee, N.K., Fok, K.W., White, A., Wilson, N.H., O'Leary, C.J., Cox, H.L., Michael, M., Yap,
1040 A.S., Cooper, H.M., 2016. Neogenin recruitment of the WAVE regulatory complex
1041 maintains adherens junction stability and tension. Nat. Commun. 7.
1042 https://doi.org/10.1038/ncomms11082
1043 Lefebvre, J.L., Sanes, J.R., Kay, J.N., 2015. Development of Dendritic Form and Function.

1044 Annu. Rev. Cell Dev. Biol. 31, 741–777. https://doi.org/10.1146/annurev-cellbio-100913-
1045 013020
1046 Machesky, L.M., Atkinson, S.J., Ampe, C., Vandekerckhove, J., Pollard, T.D., 1994. Purification
1047 of a cortical complex containing two unconventional actins from Acanthamoeba by affinity
1048 chromatography on profilin-agarose. J. Cell Biol. 127, 107–115.
1049 https://doi.org/10.1083/jcb.127.1.107
1050 Machesky, L.M., Insall, R.H., 1998. Scar1 and the related Wiskott-Aldrich syndrome protein,
1051 WASP, regulate the actin cytoskeleton through the Arp2/3 complex. Curr. Biol. 8, 1347–
1052 1356. https://doi.org/10.1016/S0960-9822(98)00015-3
1053 Minkyung, B., Frank, D., Ivan, A., Justas, D., Sergey, O., Rie, L.G., Jue, W., Qian, C., N., K.L.,
1054 Dustin, S.R., Claudia, M., Hahnbeom, P., Carson, A., R., G.C., Andy, D., H., P.J., V., R.A.,
1055 A., van D.A., C., E.A., J., O.D., Theo, S., Christoph, B., Tea, P.-K., K., R.M., Udit, D., K.,
1056 Y.C., E., B.J., Christopher, G.K., V., G.N., D., A.P., J., R.R., David, B., 2021. Accurate
1057 prediction of protein structures and interactions using a three-track neural network. Science
1058 (80-.). 373, 871–876. https://doi.org/10.1126/science.abj8754
1059 Miyoshi, T., Tsuji, T., Higashida, C., Hertzog, M., Fujita, A., Narumiya, S., Scita, G., Watanabe,
1060 N., 2006. Actin turnover-dependent fast dissociation of capping protein in the dendritic
1061 nucleation actin network: Evidence of frequent filament severing. J. Cell Biol. 175, 947–
1062 955. https://doi.org/10.1083/jcb.200604176
1063 Mudry, R.E., Perry, C.N., Richards, M., Fowler, V.M., Gregorio, C.C., 2003. The interaction of
1064 tropomodulin with tropomyosin stabilizes thin filaments in cardiac myocytes. J. Cell Biol.
1065 162, 1057–1068. https://doi.org/10.1083/jcb.200305031
1066 Narvaez-Ortiz, H.Y., Nolen, B.J., 2022. Unconcerted conformational changes in Arp2/3 complex

1067 integrate multiple activating signals to assemble functional actin networks. Curr. Biol. 32,
1068 975-987.e6. https://doi.org/10.1016/j.cub.2022.01.004
1069 Olive, C., Ibanez, L., Farias, F.H.G., Wang, F., John, P., Norton, J.B., Gentsch, J., Morris, J.C.,
1070 Li, Z., Del-aguila, J., Bergmann, K., Bradley, J., Benitez, B.A., Harari, O., Fagan, A.,
1071 Ances, B., Cruchaga, C., Victoria, M., 2020. Examination of the Effect of Rare Variants in
1072 TREM2, ABI3, and PLCG2 in LOAD Through Multiple Phenotypes. J. Alzheimers Dis. 77,
1073 1469–1482. https://doi.org/10.3233/JAD-200019.Examination
1074 Pilpel, Y., Segal, M., 2005. Rapid WAVE dynamics in dendritic spines of cultured hippocampal
1075 neurons is mediated by actin polymerization. J. Neurochem. 95, 1401–1410.
1076 https://doi.org/10.1111/j.1471-4159.2005.03467.x
1077 Polesskaya, A., Boutillon, A., Yang, S., Wang, Y., Romero, S., Liu, Y., Lavielle, M., Vacher, S.,
1078 Schnitzler, A., Molinie, N., Rocques, N., Fokin, A., Guérois, R., Bièche, I., Chen, B.,
1079 David, N.B., Gautreau, A.M., 2021. CYFIP2-containing WAVE complexes inhibit cell
1080 migration by a competition mechanism. bioRxiv 2020.07.02.184655.
1081 Pollard, T.D., 2010. A Guide to Simple and Informative Binding Assays. Mol. Biol. Cell 21,
1082 4061–4067. https://doi.org/10.1091/mbc.e10-08-0683
1083 Pollard, T.D., 2007. Regulation of Actin Filament Assembly by Arp2/3 Complex and Formins.
1084 Annu. Rev. Biophys. Biomol. Struct. 36, 451–477.
1085 https://doi.org/10.1146/annurev.biophys.35.040405.101936
1086 Pollitt, A.Y., Insall, R.H., 2009. WASP and SCAR/WAVE proteins: the drivers of actin
1087 assembly. J. Cell Sci. 122, 2575–2578. https://doi.org/10.1242/jcs.023879
1088 Racz, B., Weinberg, R.J., 2008. Organization of the Arp2/3 Complex in Hippocampal Spines. J.
1089 Neurosci. 28, 5654–5659. https://doi.org/10.1523/jneurosci.0756-08.2008

1090 Rottner, K., Stradal, T.E.B., Chen, B., 2021. WAVE regulatory complex. Curr. Biol. 31, R512–
1091 R517. https://doi.org/10.1016/j.cub.2021.01.086
1092 Scott, E.K., Luo, L., 2001. How do dendrites take their shape? Nat. Neurosci. 4, 359–365.
1093 https://doi.org/10.1038/86006
1094 Shi, R., Kramer, D.A., Chen, B., Shen, K., 2021. A two-step actin polymerization mechanism
1095 drives dendrite branching. Neural Dev. 16, 1–16. https://doi.org/10.1186/s13064-021-
1096 00154-0
1097 Shimojima Yamamoto, K., Yanagishita, T., Yamamoto, H., Miyamoto, Y., Nagata, M., Ishihara,
1098 Y., Miyashita, Y., Asano, Y., Sakata, Y., Yamamoto, T., 2021. Recurrent de novo
1099 pathogenic variant of WASF1 in a Japanese patient with neurodevelopmental disorder with
1100 absent language and variable seizures. Hum. Genome Var. 8, 2–4.
1101 https://doi.org/10.1038/s41439-021-00176-4
1102 Sims, R., Van Der Lee, S.J., Naj, A.C., Bellenguez, C., Badarinarayan, N., Jakobsdottir, J.,
1103 Kunkle, B.W., Boland, A., Raybould, R., Bis, J.C., Martin, E.R., Grenier-Boley, B.,
1104 Heilmann-Heimbach, S., Chouraki, V., Kuzma, A.B., Sleegers, K., Vronskaya, M., Ruiz,
1105 A., Graham, R.R., Olaso, R., Hoffmann, P., Grove, M.L., Vardarajan, B.N., Hiltunen, M.,
1106 Nöthen, M.M., White, C.C., Hamilton-Nelson, K.L., Epelbaum, J., Maier, W., Choi, S.H.,
1107 Beecham, G.W., Dulary, C., Herms, S., Smith, A. V., Funk, C.C., Derbois, C., Forstner,
1108 A.J., Ahmad, S., Li, H., Bacq, D., Harold, D., Satizabal, C.L., Valladares, O., Squassina, A.,
1109 Thomas, R., Brody, J.A., Qu, L., Sánchez-Juan, P., Morgan, T., Wolters, F.J., Zhao, Y.,
1110 Garcia, F.S., Denning, N., Fornage, M., Malamon, J., Naranjo, M.C.D., Majounie, E.,
1111 Mosley, T.H., Dombroski, B., Wallon, D., Lupton, M.K., Dupuis, J., Whitehead, P.,
1112 Fratiglioni, L., Medway, C., Jian, X., Mukherjee, S., Keller, L., Brown, K., Lin, H.,

Cantwell, L.B., Panza, F., McGuinness, B., Moreno-Grau, S., Burgess, J.D., Solfrizzi, V., Proitsi, P., Adams, H.H., Allen, M., Seripa, D., Pastor, P., Cupples, L.A., Price, N.D., Hannequin, D., Frank-García, A., Levy, D., Chakrabarty, P., Caffarra, P., Giegling, I., Beiser, A.S., Giedraitis, V., Hampel, H., Garcia, M.E., Wang, X., Lannfelt, L., Mecocci, P., Eiriksdottir, G., Crane, P.K., Pasquier, F., Boccardi, V., Henández, I., Barber, R.C., Scherer, M., Tarraga, L., Adams, P.M., Leber, M., Chen, Y., Albert, M.S., Riedel-Heller, S., Emilsson, V., Beekly, D., Braae, A., Schmidt, R., Blacker, D., Masullo, C., Schmidt, H., Doody, R.S., Spalletta, G., Jr, W.T.L., Fairchild, T.J., Bossù, P., Lopez, O.L., Frosch, M.P., Sacchinelli, E., Ghetti, B., Yang, Q., Huebinger, R.M., Jessen, F., Li, S., Kamboh, M.I., Morris, J.C., Sotolongo-Grau, O., Katz, M.J., Corcoran, C., Dunstan, M., Braddel, A., Thomas, C., Meggy, A., Marshall, R., Gerrish, A., Chapman, J., Aguilar, M., Taylor, S., Hill, M., Fairén, M.D., Hodges, A., Vellas, B., Soininen, H., Kloszewska, I., Daniilidou, M., Uphill, J., Patel, Y., Hughes, J.T., Lord, J., Turton, J., Hartmann, A.M., Cecchetti, R., Fenoglio, C., Serpente, M., Arcaro, M., Caltagirone, C., Orfei, M.D., Ciaramella, A., Pichler, S., Mayhaus, M., Gu, W., Lleó, A., Fortea, J., Blesa, R., Barber, I.S., Brookes, K., Cupidi, C., Maletta, R.G., Carrell, D., Sorbi, S., Moebus, S., Urbano, M., Pilotto, A., Kornhuber, J., Bosco, P., Todd, S., Craig, D., Johnston, J., Gill, M., Lawlor, B., Lynch, A., Fox, N.C., Hardy, J., Albin, R.L., Apostolova, L.G., Arnold, S.E., Asthana, S., Atwood, C.S., Baldwin, C.T., Barnes, L.L., Barral, S., Beach, T.G., Becker, J.T., Bigio, E.H., Bird, T.D., Boeve, B.F., Bowen, J.D., Boxer, A., Burke, J.R., Burns, J.M., Buxbaum, J.D., Cairns, N.J., Cao, C., Carlson, C.S., Carlsson, C.M., Carney, R.M., Carrasquillo, M.M., Carroll, S.L., Diaz, C.C., Chui, H.C., Clark, D.G., Cribbs, D.H., Crocco, E.A., Decarli, C., Dick, M., Duara, R., Evans, D.A., Faber, K.M., Fallon, K.B., Fardo, D.W., Farlow, M.R., Ferris, S.,

Foroud, T.M., Galasko, D.R., Gearing, M., Geschwind, D.H., Gilbert, J.R., Graff-Radford, N.R., Green, R.C., Growdon, J.H., Hamilton, R.L., Harrell, L.E., Honig, L.S., Huentelman, M.J., Hulette, C.M., Hyman, B.T., Jarvik, G.P., Abner, E., Jin, L.W., Jun, G., Karydas, A., Kaye, J.A., Kim, R., Kowall, N.W., Kramer, J.H., Laferla, F.M., Lah, J.J., Leverenz, J.B., Levey, A.I., Li, G., Lieberman, A.P., Lunetta, K.L., Lyketsos, C.G., Marson, D.C., Martiniuk, F., Mash, D.C., Masliah, E., McCormick, W.C., McCurry, S.M., McDavid, A.N., McKee, A.C., Mesulam, M., Miller, B.L., Miller, C.A., Miller, J.W., Murrell, J.R., Myers, A.J., O'Bryant, S., Olichney, J.M., Pankratz, V.S., Parisi, J.E., Paulson, H.L., Perry, W., Peskind, E., Pierce, A., Poon, W.W., Potter, H., Quinn, J.F., Raj, A., Raskind, M., Reisberg, B., Reitz, C., Ringman, J.M., Roberson, E.D., Rogaeva, E., Rosen, H.J., Rosenberg, R.N., Sager, M.A., Saykin, A.J., Schneider, J.A., Schneider, L.S., Seeley, W.W., Smith, A.G., Sonnen, J.A., Spina, S., Stern, R.A., Swerdlow, R.H., Tanzi, R.E., Thornton-Wells, T.A., Trojanowski, J.Q., Troncoso, J.C., Van Deerlin, V.M., Van Eldik, L.J., Vinters, H. V., Vonsattel, J.P., Weintraub, S., Welsh-Bohmer, K.A., Wilhelmsen, K.C., Williamson, J., Wingo, T.S., Woltjer, R.L., Wright, C.B., Yu, C.E., Yu, L., Garzia, F., Golamaully, F., Septier, G., Engelborghs, S., Vandenberghe, R., De Deyn, P.P., Fernadez, C.M., Benito, Y.A., Thonberg, H., Forsell, C., Lilius, L., Kinhult-Stählbom, A., Kilander, L., Brundin, R., Concari, L., Helisalmi, S., Koivisto, A.M., Haapasalo, A., Dermecourt, V., Fievet, N., Hanon, O., Dufouil, C., Brice, A., Ritchie, K., Dubois, B., Himali, J.J., Keene, C.D., Tschanz, J., Fitzpatrick, A.L., Kukull, W.A., Norton, M., Aspelund, T., Larson, E.B., Munger, R., Rotter, J.I., Lipton, R.B., Bullido, M.J., Hofman, A., Montine, T.J., Coto, E., Boerwinkle, E., Petersen, R.C., Alvarez, V., Rivadeneira, F., Reiman, E.M., Gallo, M., O'Donnell, C.J., Reisch, J.S., Bruni, A.C., Royall, D.R., Dichgans, M., Sano, M.,

1159 Galimberti, D., St George-Hyslop, P., Scarpini, E., Tsuang, D.W., Mancuso, M.,
1160 Bonuccelli, U., Winslow, A.R., Daniele, A., Wu, C.K., Peters, O., Nacmias, B.,
1161 Riemenschneider, M., Heun, R., Brayne, C., Rubinsztein, D.C., Bras, J., Guerreiro, R., Al-
1162 Chalabi, A., Shaw, C.E., Collinge, J., Tsolaki, M., Clarimón, J., Sussams, R., Lovestone, S.,
1163 O'Donovan, M.C., Owen, M.J., Behrens, T.W., Mead, S., Uitterlinden, A.G., Holmes, C.,
1164 Cruchaga, C., Ingelsson, M., Bennett, D.A., Powell, J., Golde, T.E., Graff, C., De Jager,
1165 P.L., Morgan, K., Ertekin-Taner, N., Combarros, O., Psaty, B.M., Passmore, P., Younkin,
1166 S.G., Berr, C., Gudnason, V., Rujescu, D., Dickson, D.W., Dartigues, J.F., Destefano, A.L.,
1167 Ortega-Cubero, S., Hakonarson, H., Campion, D., Boada, M., Kauwe, J.K., Farrer, L.A.,
1168 Van Broeckhoven, C., Ikram, M.A., Jones, L., Haines, J.L., Tzourio, C., Tzourio, C.,
1169 Escott-Price, V., Mayeux, R., Deleuze, J.F., Amin, N., Goate, A.M., Pericak-Vance, M.A.,
1170 Amouyel, P., Van Duijn, C.M., Ramirez, A., Wang, L.S., Lambert, J.C., Seshadri, S.,
1171 Williams, J., Schellenberg, G.D., 2017. Rare coding variants in PLCG2, ABI3, and TREM2
1172 implicate microglial-mediated innate immunity in Alzheimer's disease. Nat. Genet. 49,
1173 1373–1384. https://doi.org/10.1038/ng.3916
1174 Soderling, S.H., Langeberg, L.K., Soderling, J.A., Davee, S.M., Simerly, R., Raber, J., Scott,
1175 J.D., 2003. Loss of WAVE-1 causes sensorimotor retardation and reduced learning and
1176 memory in mice. Proc. Natl. Acad. Sci. 100, 1723–1728.
1177 https://doi.org/10.1073/pnas.0438033100
1178 Spudich, J.A., Watt, S., 1971. The Regulation of Rabbit Skeletal Muscle Contraction. J. Biol.
1179 Chem. 246, 4866–4871. https://doi.org/10.1016/s0021-9258(18)62016-2
1180 Srivastava, S., Macke, E.L., Swanson, L.C., Coulter, D., Klee, E.W., Mullegama, S. V., Xie, Y.,
1181 Lanpher, B.C., Bedoukian, E.C., Skraban, C.M., Villard, L., Milh, M., Leppert, M.L.O.,

1182 Cohen, J.S., 2021. Expansion of the genotypic and phenotypic spectrum of wasf1-related
1183 neurodevelopmental disorder. Brain Sci. 11, 1–10.
1184 https://doi.org/10.3390/brainsci11070931
1185 Takenawa, T., Suetsugu, S., 2007. The WASP-WAVE protein network: Connecting the
1186 membrane to the cytoskeleton. Nat. Rev. Mol. Cell Biol. 8, 37–48.
1187 https://doi.org/10.1038/nrm2069
1188 Tavosanis, G., 2012. Dendritic structural plasticity. Dev. Neurobiol. 72, 73–86.
1189 https://doi.org/10.1002/dneu.20951
1190 Turjanski, A.G., Gutkind, J.S., Best, R.B., Hummer, G., 2008. Binding-Induced Folding of a
1191 Natively Unstructured Transcription Factor. PLOS Comput. Biol. 4, e1000060.
1192 Wang, W., Lo, K.W.-H., Kan, H.-M., Fan, J.-S., Zhang, M., 2003. Structure of the monomeric 8-
1193 kDa dynein light chain and mechanism of the domain-swapped dimer assembly. J. Biol.
1194 Chem. 278, 41491–41499. https://doi.org/10.1074/jbc.M307118200
1195 Weeds, A., Maciver, S., 1993. F-actin capping proteins. Curr. Opin. Cell Biol. 5, 63–69.
1196 https://doi.org/10.1016/S0955-0674(05)80009-2
1197 Xing, G., Li, M., Sun, Y., Rui, M., Zhuang, Y., Lv, H., Han, J., Jia, Z., Xie, W., 2018. Neurexin–
1198 neuroligin 1 regulates synaptic morphology and functions via the WAVE regulatory
1199 complex in Drosophila neuromuscular junction. Elife 7, 1–23.
1200 https://doi.org/10.7554/eLife.30457
1201 Yamazaki, D., Fujiwara, T., Suetsugu, S., Takenawa, T., 2005. A novel function of WAVE in
1202 lamellipodia: WAVE1 is required for stabilization of lamellipodial protrusions during cell
1203 spreading. Genes Cells 10, 381–392. https://doi.org/10.1111/j.1365-2443.2005.00845.x
1204 Yan, Z., Kim, E., Datta, D., Lewis, D.A., Soderling, S.H., 2016. Synaptic Actin Dysregulation, a

1205 Convergent Mechanism of Mental Disorders? J. Neurosci. 36, 11411–11417.
1206 https://doi.org/10.1523/jneurosci.2360-16.2016
1207 Zhao, A., Zhou, R., Gu, Q., Liu, M., Zhang, B., Huang, J., Yang, B., Yao, R., Wang, J., Lv, H.,
1208 Wang, J., Shen, Y., Wang, H., Chen, X., 2021. Trio exome sequencing identified a novel de
1209 novo WASF1 missense variant leading to recurrent site substitution in a Chinese patient
1210 with developmental delay, microcephaly, and early-onset seizures: a mutational hotspot
1211 p.Trp161 and literature review. Clin. Chim. Acta. https://doi.org/10.1016/j.cca.2021.08.030
1212 Zhao, B., Meka, D.P., Scharrenberg, R., König, T., Schwanke, B., Kobler, O., Windhorst, S.,
1213 Kreutz, M.R., Mikhaylova, M., Calderon de Anda, F., 2017. Microtubules Modulate F-actin
1214 Dynamics during Neuronal Polarization. Sci. Rep. 7, 9583. https://doi.org/10.1038/s41598-
1215 017-09832-8
1216 Zhou, P., Wagner, G., 2010. Overcoming the solubility limit with solubility-enhancement tags:
1217 successful applications in biomolecular NMR studies. J. Biomol. NMR 46, 23–31.
1218 https://doi.org/10.1007/s10858-009-9371-6
1219 Zou, W., Dong, X., Broederdorf, T.R., Shen, A., Kramer, D.A., Shi, R., Liang, X., Miller, D.M.,
1220 Xiang, Y.K., Yasuda, R., Chen, B., Shen, K., 2018. A Dendritic Guidance Receptor
1221 Complex Brings Together Distinct Actin Regulators to Drive Efficient F-Actin Assembly
1222 and Branching. Dev. Cell 45, 362-375.e3. https://doi.org/10.1016/j.devcel.2018.04.008
1223 Zou, W., Shen, A., Dong, X., Tugizova, M., Xiang, Y.K., Shen, K., 2016. A multi-protein
1224 receptor-ligand complex underlies combinatorial dendrite guidance choices in C. elegans.
1225 Elife 5, 1–25. https://doi.org/10.7554/elife.18345
1226 Zweier, M., Begemann, A., McWalter, K., Cho, M.T., Abela, L., Banka, S., Behring, B., Berger,
1227 A., Brown, C.W., Carneiro, M., Chen, J., Cooper, G.M., Finnila, C.R., Guillen Sacoto, M.J.,

1228 Henderson, A., Hüffmeier, U., Joset, P., Kerr, B., Lesca, G., Leszinski, G.S., McDermott,
1229 J.H., Meltzer, M.R., Monaghan, K.G., Mostafavi, R., Õunap, K., Plecko, B., Powis, Z.,
1230 Purcarin, G., Reimand, T., Riedhammer, K.M., Schreiber, J.M., Sirsi, D., Wierenga, K.J.,
1231 Wojcik, M.H., Papuc, S.M., Steindl, K., Sticht, H., Rauch, A., 2019. Spatially clustering de
1232 novo variants in CYFIP2, encoding the cytoplasmic FMRP interacting protein 2, cause
1233 intellectual disability and seizures. Eur. J. Hum. Genet. 27, 747–759.
1234 https://doi.org/10.1038/s41431-018-0331-z
1235
1236